

# Quantum Gravity and Extra Dimensions at High-Energy Colliders

Gian F. Giudice, Riccardo Rattazzi, and James D. Wells

*Theory Division, CERN  
CH-1211 Geneva 23, Switzerland*

## Abstract

Recently it has been pointed out that the characteristic quantum-gravity scale could be as low as the weak scale in theories with gravity propagating in higher dimensions. The observed smallness of Newton's constant is a consequence of the large compactified volume of the extra dimensions. We investigate the consequences of this supposition for high-energy collider experiments. We do this by first compactifying the higher dimensional theory and constructing a  $3 + 1$ -dimensional low-energy effective field theory of the graviton Kaluza-Klein excitations and their interactions with ordinary matter. We then consider graviton production processes, and select  $\gamma + \cancel{E}$  and jet +  $\cancel{E}$  signatures for careful study. We find that both a 1 TeV  $e^+e^-$  collider and the CERN LHC will be able to reliably and perturbatively probe the fundamental gravity scale up to several TeV, with the precise value depending on the number of extra dimensions. Similarly, searches at LEP2 and the Tevatron are able to probe this scale up to approximately 1 TeV. We also discuss virtual graviton exchange, which induces local dimension-eight operators associated with the square of the energy-momentum tensor. We estimate the size of such operators and study their effects on  $f\bar{f} \rightarrow \gamma\gamma$  observables.

# Contents

<b>1</b>	<b>Introduction</b>	<b>1</b>
<b>2</b>	<b>The Kaluza-Klein Excitations of the Graviton</b>	<b>7</b>
<b>3</b>	<b>Feynman Rules</b>	<b>14</b>
<b>4</b>	<b>Graviton Production Processes</b>	<b>18</b>
<b>5</b>	<b>Virtual Graviton Exchange</b>	<b>21</b>
<b>6</b>	<b>Graviton Production and Collider Experiments</b>	<b>24</b>
6.1	$e^+e^-$ and Muon Colliders . . . . .	25
6.2	Hadron Colliders . . . . .	32
<b>7</b>	<b>The Operator <math>\mathcal{T}</math> and Collider Experiments</b>	<b>40</b>
7.1	$e^+e^-$ and Muon Colliders . . . . .	43
7.2	Hadron Colliders . . . . .	45
<b>8</b>	<b>Conclusions</b>	<b>45</b>

## 1 Introduction

The idea that quantum-gravity effects appear only at energy scales near the Planck mass  $M_P = 1.2 \times 10^{19}$  GeV has been shaken recently [1, 2, 3, 4, 5]. Witten [3] has pointed out that the string scale  $M_S$  can be substantially lower than that predicted by the tree-level relation [6]

$$M_S = M_P \frac{\sqrt{k\alpha_{GUT}}}{2}. \quad (1)$$

Here  $\alpha_{GUT}$  is the unified gauge coupling constant and  $k$  is the Kač-Moody level, typically of order unity. Equation (1) predicts a value of  $M_S$  which is too large to be consistent with unification of the gauge couplings measured at low energies. Several solutions have been proposed to cure this phenomenologically unpleasant aspect of string theory: large

threshold corrections, high Kač-Moody levels, or GUT models embedded in strings (for a review, see ref. [7]). However, as pointed out in ref. [3], explicit calculations in the strong-coupling regime using string duality show that eq. (1) receives large corrections, and  $M_S$  can be lowered to values compatible with gauge coupling unification. Thus one can claim to have achieved a complete unification of gauge and gravity forces at a single energy scale, although  $M_S$  is now a model-dependent parameter, and therefore no new low-energy predictions can be derived.

The result that the string and the Planck scale are not necessarily tied together by eq. (1) has been pushed to its extreme consequences by Lykken [2]. Indeed, even in the absence of realistic models, one can speculate on the radical possibility that the string scale is as low as the Fermi scale. If this is the case, one loses the original motivation for space-time supersymmetry, based on the hierarchy problem. Supersymmetry may still be desirable as a necessary ingredient of string theory, but it could be broken at the string level and not be present in the effective low-energy field theory. For collider experiments this implies that the superparticle masses should follow a pattern of string Regge recurrences.

Arkani-Hamed, Dimopoulos, and Dvali [1] have made the very interesting proposal that, while Standard Model particles live in the usual 3+1-dimensional space, gravity can propagate in a higher-dimensional space. The relative feebleness of gravity with respect to weak forces is related to the size of the compactified extra dimensions which, in units of  $\text{TeV}^{-1}$ , is very large. Newton's constant measured in the 3+1-dimensional space can be expressed as [1]

$$G_N^{-1} = 8\pi R^\delta M_D^{2+\delta}, \quad (2)$$

where  $M_D \sim \text{TeV}$  is the fundamental mass scale,  $\delta$  is the number of extra dimensions, and  $R$  is the radius of the compactified space, here assumed to be a torus. The hierarchy problem is overcome, because there is a single fundamental mass scale  $M_D$ , to be identified with the weak scale. Since gravity forces are not well probed at distances less than a millimeter [8], eq. (2) is consistent with present measurements as long as  $\delta$  is larger than or equal to 2. Deviations from the standard Newtonian law of gravitational attraction are predicted at distances smaller than  $R \sim 10^{\frac{32}{\delta}-19}$  meters. In the case  $\delta = 2$ , such effects will be probed at future experiments, which are sensitive to gravitational forces down to distances of tens of microns.

Although the idea that our 3+1-dimensional world could be a field-theoretical topological defect of a higher-dimensional theory dates back to ref. [9], it finds a natural setting in the context of string theory. Indeed, Dirichlet branes are defects intrinsic to string theory (for reviews, see ref. [10]). Standard Model particles are naturally confined to the lower-dimensional space, since they correspond to open strings with the endpoints attached to the brane. On the other hand, gravitons correspond to closed strings which propagate in the whole higher-dimensional space. This picture of ordinary particles confined on the brane with gravity propagating in the bulk can be realized in several string models [4, 11, 12].

Recently, there has been considerable activity [11]–[26] in investigating the proposal of ref. [1] and related ones. These scenarios are undoubtedly very intriguing, although there are still many theoretical open questions. First of all, the solution to the hierarchy problem is not complete until we can predict the radius  $R$  of the compactified space. After all, the effect of eq. (2) is just to trade the small ratio  $M_W/M_P$  with the large number  $(RM_W)^{\delta/2}$ . Interesting attempts to address this problem have been presented in refs. [20, 21]. The second problem we want to mention is related to the cosmology of this scenario. During the early phase of the universe, energy can be emitted from the brane into the bulk in the form of gravitons. The gravitons propagate in the extra dimensions and can decay into ordinary particles only by interacting with the brane, and therefore with a rate suppressed by  $1/M_P^2$ . Their contribution to the present energy density exceeds the critical value unless [1]

$$T_\star < \frac{M_D}{\text{TeV}} 10^{\frac{6\delta-15}{\delta+2}} \text{MeV}. \quad (3)$$

Here  $T_\star$  is the maximum temperature to which we can simply extrapolate the thermal history of the Universe, assuming it is in a stage with completely stabilized  $R$  and with vanishing energy density in the compactified space. As a possible example of its origin,  $T_\star$  could correspond to the reheating temperature after an inflationary epoch. The bound in eq. (3) is very constraining. In particular, for  $\delta = 2$ , only values of  $M_D$  larger than about 6 TeV can lead to  $T_\star > 1$  MeV and allow for standard nucleosynthesis. Moreover, even for larger values of  $\delta$ , eq. (3) is problematic for any mechanism of baryogenesis [22].

The possibility that ordinary matter lives in a higher-dimensional space with  $\text{TeV}^{-1}$  size has also been considered in the literature [5, 23]. Low-energy supersymmetry breaking within perturbative string theory then can be related to the radius of the compactified space. Such

a point of view is not inconsistent with the previous picture. Our world would be confined to a  $d$ -dimensional space with  $d - 4$  coordinates of size  $r \sim \text{TeV}^{-1}$ , which is embedded in a  $D$ -dimensional space with extra coordinates of size  $R$  (much larger than  $r$ ) where only gravity is free to propagate. Recently, it has been argued that the Kaluza-Klein states of the Standard Model particles could be used to lower the GUT scale [24].

In summary, it does not appear implausible that quantum-gravity effects can start revealing themselves at energies much lower than  $M_P$ , possibly as low as the weak scale. This has the exciting implication that future high-energy collider experiments can directly probe the physics of quantum gravity. Above the TeV energy scale, completely new phenomena could emerge as resonant production of the Regge recurrences of string theory or excitations of Kaluza-Klein modes of ordinary particles [25].

There is little doubt that, if these scenarios have some truth, the collider phenomenology above the TeV scale would be quite distinct from Standard Model expectations. However, because of our basic ignorance about the underlying quantum-gravity theory, it is less clear what the distinguishing experimental signatures would be, and whether any of these signatures would depend only on the conceptual theoretical hypothesis and not on the specific model realization. These are the questions we want to address in this paper.

We consider the scenario of ref. [1], in which gravity can propagate into extra dimensions and define an effective theory valid below the fundamental scale  $M_D$ . As usual, the contribution of the unknown ultraviolet physics is reabsorbed in unknown coefficients of the effective theory. However, the advantage of the effective-theory approach is that it allows one to separate ultraviolet from infrared contributions and therefore to derive some model-independent results, which are affected only by the infrared behaviour. In particular, we will argue that rates for graviton production are model independent, as long as the typical energy is less than  $M_D$ .

Let us consider the form of the effective theory below  $M_D$ . The dynamical degrees of freedom are described by the Standard Model particles, by the graviton, and by possible other light fields related to the brane dynamics [26]. In particular, the  $Y$  modes describing the deformations of the brane in the  $D$ -dimensional space could be much lighter than  $M_D$  or even massless, if the brane breaks translation invariance in the transverse directions only spontaneously. The modes  $Y$  are coupled to ordinary matter only in pairs and therefore their

production cross-section is subleading with respect to the case of gravitons, which are singly produced. Thus we will disregard these fields. Indeed, for simplicity, we can just assume that the brane is rigid with its position fixed, and the  $Y$  fields have masses of order  $M_D$  or larger. For instance, this case arises when the Standard Model degrees of freedom live at an orbifold singularity.

The graviton corresponds to the excitations of the  $D$ -dimensional metric. In terms of 4-dimensional indices, the metric tensor contains spin-2, spin-1, and spin-0 particles. Moreover, since these fields depend on  $D$ -dimensional coordinates, they can be expressed as a tower of Kaluza-Klein modes. The mass of each Kaluza-Klein mode corresponds to the modulus of its momentum in the direction transverse to the brane. The picture of a massless graviton propagating in  $D$  dimensions and the picture of massive Kaluza-Klein gravitons propagating in 4 dimensions are equivalent, and we will often use both descriptions in our discussion.

In the low-energy limit, the coupling of the Kaluza-Klein gravitons with the particles on the brane is determined by general covariance both in the full  $D$ -dimensional theory and in the 4-dimensional brane description. At lowest order this means that the metric on the brane is simply the bulk metric projected to the 4 dimensions parallel to the brane. An important consequence is then the universal nature of the coupling of the Kaluza-Klein modes.

At lowest order in  $1/M_P$  the above remark is sufficient to predict the emission rates of real gravitons in the effective theory. In this way we can calculate the experimental signal expected at high-energy colliders and can compare it with the Standard Model background. This provides a rather model-independent test of the idea that gravity can propagate in extra dimensions. Effectively here we are studying quantum gravity in its weak-coupling regime, where we can make definite predictions, and we are determining its behaviour before the onset of the fundamental underlying theory.

It may seem hopeless to observe processes with real graviton emission, since the relevant interaction is suppressed by inverse powers of  $M_P$ . However, the large phase space of the Kaluza-Klein modes, corresponding to the large volume of the compactified space exactly cancels the dependence on  $M_P$  and gives an effective interaction suppressed only by inverse powers of  $M_D$  (see sect. 4). In the  $D$ -dimensional language this is evident, since the graviton interactions are determined by the only available scale  $M_D$ . Therefore, for collider applications, we can work in the limit of infinite compactified space ( $R \rightarrow \infty$ ) in which the graviton

Kaluza-Klein excitations have a continuous spectrum, and the usual four-dimensional gravitational effects are shut off.

An important remark is that we have to be aware that other effects inherent to the fundamental theory, and therefore not computable with an effective Lagrangian approach, can give various experimental signals. These effects could be more easily detectable than the effects we are studying. Therefore the discovery modes could be different than what is discussed here. However, these will be model-dependent effects, and little can be said about them with sufficient generality at present. The specific experimental processes discussed here can provide a handle to disentangle unexpected signals and test a precise hypothesis. Moreover, in case no deviation from the Standard Model is observed, they define in a quantitative way the strategy to obtain lower bounds on the new physics energy scale.

Another remark concerns the value of the ultraviolet validity cutoff of the effective theory. In practice, this is an important issue, because this cutoff determines the maximum energy to which we can extrapolate our predictions and, analogously, the minimum value of  $M_D$  which can be studied reliably at a collider experiment. This energy cutoff is expected to be of order  $M_D$ . As we will show in sect. 4 and 5, naive dimensional analysis and unitarity arguments suggest that the effective theory could be valid up to energies quite larger than  $M_D$ . In reality it is more reasonable to believe that the fundamental theory that regularizes quantum gravity sets in well before the latter becomes strongly interacting. In the context of string theory, the belief is that the string scale is smaller than  $M_D$ , and therefore our effective theory has a more limited applicability energy range, although large enough to be used for collider predictions, as we will illustrate in the sect. 6. It is also possible that the fundamental theory of gravity introduces new phenomena at scales equal to or less than  $M_D$  but does not significantly corrupt the graviton-emission signals up to larger energy scales.

The remainder of the paper is organized as follows. In sect. 2 we introduce the graviton Kaluza-Klein modes and identify the physical degrees of freedom. In sect. 3 we derive the graviton Feynman rules necessary for our calculation. The cross-sections for graviton production and for processes mediated by virtual-graviton exchange are computed in sects. 4 and 5. The analysis of the observability of graviton signals at future high-energy colliders is contained in sects. 6 and 7.

## 2 The Kaluza-Klein Excitations of the Graviton

In this section we study the equations that describe the Kaluza-Klein excitations of the graviton and identify the physical degrees of freedom in the effective theory. At low energy and small curvature the equations of motion of the effective theory reduce to the Einstein equation in  $D = 4 + \delta$  dimensions

$$\mathcal{G}_{AB} \equiv \mathcal{R}_{AB} - \frac{1}{2}g_{AB}\mathcal{R} = -\frac{T_{AB}}{\bar{M}_D^{2+\delta}} \quad A, B = 1, \dots, D, \quad (4)$$

where  $\bar{M}_D$  is the reduced Planck mass of the  $D$ -dimensional theory.

In general, the presence of the brane on which we live will create a non-trivial  $D$ -dimensional metric background. However, it is quite reasonable to expect that the brane surface tension  $f^4$  does not exceed the fundamental scale  $M_D^4$ . Therefore, when the distance from the brane gets much bigger than  $1/M_D$ , the metric  $g_{AB}$  will be essentially flat. Correspondingly, if we study the emission of “soft” gravitons, with a momentum transverse to the brane  $q_T \ll M_D$ , we are only concerned with distances at which the metric is essentially flat\*. In view of the above remark, we expand the metric  $g_{AB}$  around its Minkowski value  $\eta_{AB}$

$$g_{AB} = \eta_{AB} + 2\bar{M}_D^{-1-\delta/2}h_{AB}. \quad (5)$$

Keeping only the first power of  $h$ , eq. (4) becomes

$$\begin{aligned} \bar{M}_D^{1+\delta/2}\mathcal{G}_{AB} &= \square h_{AB} - \partial_A\partial^C h_{CB} - \partial_B\partial^C h_{CA} + \partial_A\partial_B h_C^C \\ &- \eta_{AB}\square h_C^C + \eta_{AB}\partial^C\partial^D h_{CD} = -\bar{M}_D^{-1-\delta/2}T_{AB}, \end{aligned} \quad (6)$$

where indices are raised or lowered using the flat-space metric and summation over repeated indices is understood.

A point in the  $D$ -dimensional space is described by the set of coordinates  $z = (z_1, \dots, z_D)$ . Let us explicitly separate the ordinary four-dimensional coordinates from the extra dimensional ones,

$$z = (x, y) \quad x = (x_0, \vec{x}), \quad y = (y_1, \dots, y_\delta), \quad \delta = D - 4. \quad (7)$$

---

\*We thank Raman Sundrum for important comments on this issue, see also ref. [20].

We now demand periodicity of the fields under the following translation in the compactified space

$$y_j \rightarrow y_j + 2\pi R \quad j = 1, \dots, \delta, \quad (8)$$

where  $R$  is the compactification radius. For simplicity we assume that the compactified space is a torus, but our considerations are valid for different compact spaces. Equation (8) implies

$$h_{AB}(z) = \sum_{n_1=-\infty}^{+\infty} \dots \sum_{n_\delta=-\infty}^{+\infty} \frac{h^{(n)}_{AB}(x)}{\sqrt{V_\delta}} e^{i\frac{n^j y_j}{R}}, \quad (9)$$

where  $n = (n_1, \dots, n_\delta)$  and  $V_\delta$  is the volume of the compactified space,

$$V_\delta = (2\pi R)^\delta. \quad (10)$$

The tensor  $h(z)$  has been split into an infinite sum of Kaluza-Klein modes  $h^{(n)}(x)$  which live in the four-dimensional space.

We assume that ordinary matter is confined on the brane, and therefore, in the limit of weak gravitational field, the energy-momentum tensor becomes

$$T_{AB}(z) = \eta_A^\mu \eta_B^\nu T_{\mu\nu}(x) \delta(y) \quad \mu, \nu = 0, \dots, 3. \quad (11)$$

The singularity of the  $\delta$  function in eq. (11) will presumably be smoothed by effects of the finite brane-size in the transverse direction. However, these effects are important only in the short-distance regime. For our purposes, eq. (11) means that the Kaluza-Klein modes of the energy-momentum tensor are independent of  $n$ , in the low-energy region, where  $n$  is smaller than  $\bar{M}_D R$ . This is a crucial ingredient of our analysis, since it entails a universal coupling of all relevant Kaluza-Klein gravitons to ordinary matter, thus allowing us to make definite predictions on their production cross-sections.

Notice that eq. (11) can more formally be obtained via the induced metric  $\hat{g}_{\mu\nu}$  on the brane

$$\hat{g}_{\mu\nu}(x) = g_{AB}[Y(x)] \partial_\mu Y^A(x) \partial_\nu Y^B(x) \quad (12)$$

where  $Y^A$  are the background fields describing the position of the brane. The metric  $\hat{g}$  measures distances on the brane and should be used to write a covariant action. In the

static gauge ( $Y^\mu = x^\mu$  for  $\mu = 0, \dots, 3$  and  $Y_i = 0$  for  $i = 4, \dots, D - 1$ ) one simply has  $\hat{g}_{\mu\nu} = g_{\mu\nu}$ , and the above coupling to bulk  $(\mu, \nu)$  gravitons follows.

We should recall that in general there could also be couplings to  $(i, j)$  gravitons (polarized orthogonal to the brane). In particular, the fields  $Y^i$ , if dynamical, couple to gravitons via  $h_{ij}\partial_\mu Y^i\partial_\nu Y^j\eta^{\mu\nu}$ . Moreover, in the case of D-branes there are also fermions (the partners of  $Y^i$ ) that couple to the perpendicularly polarized gravitons  $h_{ij}$ , while gauge bosons obviously cannot. The coupling to  $h_{ij}$  is evidently model dependent, and it does not seem inconsistent to assume that it vanishes for the Standard Model degrees of freedom. This is the assumption underlying eq. (11) and the rest of our analysis.

In the context of D-branes, there exist interesting papers discussing the emission and absorption of gravitons by the brane [27, 28]. In this case, using string theory, one can even perform the calculation in the high-energy region, where  $\sqrt{s}$  is larger than the string scale. It is worth pointing out that the low-energy (soft gravitons) limit of that calculation agrees with the result obtained by an effective theory, where the bulk gravitons propagate in a flat background and couple to the fields on the brane via the induced metric [27].

Let us now go back to the equations of motion. After multiplying both sides of the Kaluza-Klein expansion of eq. (6) by  $e^{-i\frac{y}{R}}$  and integrating over the extra-dimensional coordinates, we obtain the following set of equations:

$$\begin{aligned} \mathcal{G}^{(n)}_{\mu\nu}(x) &\equiv (\square + \hat{n}^2)h^{(n)}_{\mu\nu} - \left[ \partial_\mu\partial_\lambda h^{(n)\lambda}_\nu + i\hat{n}_j\partial_\mu h^{(n)j}_\nu + (\mu \leftrightarrow \nu) \right] + \\ &\quad \left[ \partial_\mu\partial_\nu - \eta_{\mu\nu}(\square + \hat{n}^2) \right] \left[ h^{(n)\lambda}_\lambda + h^{(n)j}_j \right] + \\ &\quad \eta_{\mu\nu} \left[ \partial^\lambda\partial^\sigma h^{(n)}_{\lambda\sigma} + 2i\hat{n}_j\partial^\lambda h^{(n)j}_\lambda - \hat{n}^j\hat{n}^k h^{(n)}_{jk} \right] = -\frac{T_{\mu\nu}}{M_P}, \end{aligned} \quad (13)$$

$$\begin{aligned} \mathcal{G}^{(n)}_{\mu j}(x) &\equiv (\square + \hat{n}^2)h^{(n)}_{\mu j} - \partial_\mu\partial_\nu h^{(n)\nu}_j - i\hat{n}_k\partial_\mu h^{(n)k}_j - i\hat{n}_j\partial_\nu h^{(n)\nu}_\mu \\ &\quad + \hat{n}_j\hat{n}_k h^{(n)k}_\mu + i\hat{n}_j\partial_\mu \left[ h^{(n)\nu}_\nu + h^{(n)k}_k \right] = 0, \end{aligned} \quad (14)$$

$$\begin{aligned} \mathcal{G}^{(n)}_{jk}(x) &\equiv (\square + \hat{n}^2)h^{(n)}_{jk} - \left[ i\hat{n}_j\partial_\mu h^{(n)\mu}_k - \hat{n}_j\hat{n}_\ell h^{(n)\ell}_k + (j \leftrightarrow k) \right] \\ &\quad - \left[ \hat{n}_j\hat{n}_k + \eta_{jk}(\square + \hat{n}^2) \right] \left[ h^{(n)\mu}_\mu + h^{(n)\ell}_\ell \right] + \\ &\quad \eta_{jk} \left[ \partial^\mu\partial^\nu h^{(n)}_{\mu\nu} + 2i\hat{n}_\ell\partial^\mu h^{(n)\ell}_\mu - \hat{n}^\ell\hat{n}^m h^{(n)}_{\ell m} \right] = 0. \end{aligned} \quad (15)$$

Here the D'Alambertian operator acts on the four-dimensional space  $\square = \partial^\mu \partial_\mu$ , and we have defined<sup>†</sup>  $\hat{n} \equiv n/R$ ,  $\hat{n}^2 \equiv -\hat{n}^j \hat{n}_j = \sum_{j=1}^{\delta} |\hat{n}_j|^2$ . We can now interpret the quantity

$$\bar{M}_P \equiv \sqrt{V_\delta} \bar{M}_D^{1+\delta/2} = (2\pi R)^{\delta/2} \bar{M}_D^{1+\delta/2} \equiv R^{\delta/2} M_D^{1+\delta/2} \quad (16)$$

as the ordinary reduced Planck mass,  $\bar{M}_P = M_P/\sqrt{8\pi} = 2.4 \times 10^{18}$  GeV. For future convenience we have also defined the  $D$ -dimensional Planck mass, related to the reduced Planck mass, by the equation  $M_D = (2\pi)^{\delta/(2+\delta)} \bar{M}_D$ . With eq. (16) we have rederived, using the point of view of general relativity, the relation (2) between  $M_P$  and  $M_D$  previously obtained in ref. [1].

In order to solve the system of coupled differential equations it is convenient to rewrite them in terms of the following new dynamical variables:

$$G^{(n)}_{\mu\nu} \equiv h^{(n)}_{\mu\nu} + \frac{\kappa}{3} \left( \eta_{\mu\nu} + \frac{\partial_\mu \partial_\nu}{\hat{n}^2} \right) H^{(\bar{n})} - \partial_\mu \partial_\nu P^{(n)} + \partial_\mu Q^{(n)}_{\nu} + \partial_\nu Q^{(n)}_{\mu} \quad (17)$$

$$V^{(n)}_{\mu j} \equiv \frac{1}{\sqrt{2}} \left[ i h^{(n)}_{\mu j} - \partial_\mu P^{(n)}_j - \hat{n}_j Q^{(n)}_{\mu} \right] \quad (18)$$

$$S^{(n)}_{jk} \equiv h^{(n)}_{jk} - \frac{\kappa}{\delta-1} \left( \eta_{jk} + \frac{\hat{n}_j \hat{n}_k}{\hat{n}^2} \right) H^{(\bar{n})} + \hat{n}_j P^{(n)}_k + \hat{n}_k P^{(n)}_j - \hat{n}_j \hat{n}_k P^{(n)} \quad (19)$$

$$H^{(\bar{n})} \equiv \frac{1}{\kappa} \left[ h^{(n)j}_j + \hat{n}^2 P^{(n)} \right] \quad (20)$$

$$Q^{(n)}_{\mu} \equiv -i \frac{\hat{n}_j}{\hat{n}^2} h^{(n)j}_{\mu} \quad (21)$$

$$P^{(n)}_j \equiv \frac{\hat{n}_k}{\hat{n}^2} h^{(n)k}_j + \hat{n}_j P^{(n)} \quad (22)$$

$$P^{(n)} \equiv \frac{\hat{n}^j \hat{n}^k}{\hat{n}^4} h^{(n)}_{jk}. \quad (23)$$

The degrees of freedom contained in  $G^{(n)}_{\mu\nu}$ ,  $V^{(n)}_{\mu j}$ ,  $S^{(n)}_{jk}$ ,  $H^{(\bar{n})}$ ,  $Q^{(n)}_{\mu}$ ,  $P^{(n)}_j$ ,  $P^{(n)}$  correctly match the number of degrees of freedom in  $h_{AB}$  without giving a redundant description, because of the identities  $\hat{n}^j V^{(n)}_{\mu j} = 0$ ,  $\hat{n}^j S^{(n)}_{jk} = 0$ ,  $S^{(n)j}_j = 0$ ,  $\hat{n}^j P^{(n)}_j = 0$ . For convenience, we choose

$$\kappa = \sqrt{\frac{3(\delta-1)}{\delta+2}}, \quad (24)$$

---

<sup>†</sup>In our conventions, the flat metric is  $\eta_{\mu\nu} = \text{diag}(+, -, -, -)$  and  $\eta_{jk} = -\delta_{jk}$ .

in order to have a canonical normalization of the field  $H^{(\vec{n})}$ . Notice that, for  $\delta = 1$ , our parametrization is singular, since the fields  $P^{(n)}_j$ ,  $P^{(n)}$ , and  $H^{(\vec{n})}$  are no longer independent. However, we will be interested only in the case  $\delta > 1$ .

By contracting the free indices of eqs. (13)–(15) either with the flat metric tensor or with  $\partial^\mu$  and  $\hat{n}^j$  ( $j = 1, \dots, \delta$ ), we obtain three constraints<sup>‡</sup> on the Kaluza-Klein components of the tensor  $h$  ( $n \neq 0$ ):

$$\partial^\mu G^{(n)}_{\mu\nu} = \frac{\partial_\nu T^\mu_\mu}{3\hat{n}^2 \bar{M}_P} \quad (25)$$

$$G^{(n)\mu}_\mu = \frac{T^\mu_\mu}{3\hat{n}^2 \bar{M}_P} \quad (26)$$

$$\partial^\mu V^{(n)}_{\mu j} = 0. \quad (27)$$

Replacing in eqs. (13)–(15) the constraints given in eqs. (25)–(27), we can rewrite the equations of motion for each of the Kaluza-Klein modes  $n \neq 0$  as

$$(\square + \hat{n}^2) G^{(n)}_{\mu\nu} = \frac{1}{\bar{M}_P} \left[ -T_{\mu\nu} + \left( \frac{\partial_\mu \partial_\nu}{\hat{n}^2} + \eta_{\mu\nu} \right) \frac{T^\lambda_\lambda}{3} \right] \quad (28)$$

$$(\square + \hat{n}^2) V^{(n)}_{\mu j} = 0 \quad (29)$$

$$(\square + \hat{n}^2) S^{(n)}_{jk} = 0 \quad (30)$$

$$(\square + \hat{n}^2) H^{(\vec{n})} = \frac{\kappa}{3\bar{M}_P} T^\mu_\mu. \quad (31)$$

These equations show that only  $G^{(n)}_{\mu\nu}$ ,  $V^{(n)}_{\mu j}$ ,  $S^{(n)}_{jk}$ ,  $H^{(\vec{n})}$  describe propagating particles, while  $Q^{(n)}_\mu$ ,  $P^{(n)}_j$ ,  $P^{(n)}$  do not appear in the equations of motions. This result can be understood by studying the transformation properties of the different fields under coordinate reparametrization. Let us consider a general coordinate transformation

$$z_A \rightarrow z'_A = z_A + \epsilon_A(z), \quad (32)$$

where  $\partial_B \epsilon_A$  is at most of the same order of magnitude as  $h_{AB}$ . This transformation induces a variation of the metric such that

$$\delta_\epsilon h_{AB} = -\partial_A \epsilon_B - \partial_B \epsilon_A. \quad (33)$$

---

<sup>‡</sup>The constraints come from the equations  $\mathcal{G}^{(n)\mu}_\mu = -T^\mu_\mu/\bar{M}_P$ ,  $\partial^\mu \mathcal{G}^{(n)}_{\mu\nu} = 0$ , and  $\hat{n}^j \mathcal{G}^{(n)}_{jk} = 0$ . Notice that the conditions  $\hat{n}^j \mathcal{G}^{(n)}_{\mu j} = 0$  and  $\partial^\mu \mathcal{G}^{(n)}_{\mu j} = 0$  do not provide further constraints because they identically follow from the previous equations and energy-momentum conservation in  $D$  dimensions. Finally the information of the equation  $\mathcal{G}^{(n)j}_j = 0$  is directly contained in the equations of motion.

Using a Kaluza-Klein mode expansion for the gauge parameter  $\epsilon$

$$\epsilon_A(z) = \sum_{n_1=-\infty}^{+\infty} \dots \sum_{n_\delta=-\infty}^{+\infty} \epsilon^{(n)}{}_A(x) e^{i \frac{n^j y_j}{R}}, \quad (34)$$

the diffeomorphism in eq. (33) induces the following transformation laws for the fields defined in eqs. (17)–(23),

$$\delta_\epsilon G^{(n)}{}_{\mu\nu} = 0, \quad \delta_\epsilon V^{(n)}{}_{\mu j} = 0, \quad \delta_\epsilon S^{(n)}{}_{jk} = 0, \quad \delta_\epsilon H^{(\vec{n})} = 0, \quad (35)$$

$$\delta_\epsilon Q^{(n)}{}_\mu = \frac{1}{2} \partial_\mu \delta_\epsilon P^{(n)} + \epsilon^{(n)}{}_\mu \quad (36)$$

$$\delta_\epsilon P^{(n)}{}_j = -\frac{1}{2} \hat{n}_j \delta P^{(n)} - i \epsilon^{(n)}{}_j \quad (37)$$

$$\delta_\epsilon P^{(n)} = 2i \frac{\hat{n}_j}{\hat{n}^2} \epsilon^{(n)j}. \quad (38)$$

Thus, while  $G^{(n)}{}_{\mu\nu}, V^{(n)}{}_{\mu j}, S^{(n)}{}_{jk}, H^{(\vec{n})}$  are gauge-invariant fields,  $Q^{(n)}{}_\mu, P^{(n)}{}_j, P^{(n)}$  are gauge-dependent and do not describe physical particles. In particular, they can all be simultaneously set to zero at any four-dimensional space-time point for any  $n \neq 0$ . We will refer to the gauge choice in which  $Q^{(n)}{}_\mu = 0, P^{(n)}{}_j = 0, P^{(n)} = 0$  as the unitary gauge.

We now want to identify the physical content of the gauge-invariant fields. The free propagation of  $G^{(n)}{}_{\mu\nu}$  is given by eqs. (25) and (28) in the limit  $T_{\mu\nu} = 0$ ,

$$\left(\square + \hat{n}^2\right) G^{(n)}{}_{\mu\nu} = 0 \quad (39)$$

$$\partial^\mu G^{(n)}{}_{\mu\nu} = 0 \quad (40)$$

$$G^{(n)\mu}{}_\mu = 0. \quad (41)$$

Equation (39) describes the free propagation of the bosonic modes  $G^{(n)}{}_{\mu\nu}$  having squared masses equal to  $\hat{n}^2$ . For any given  $n$ , the constraints in eqs. (40)–(41) eliminate 5 degrees of freedom out of the 10 contained in the symmetric tensor  $G^{(n)}{}_{\mu\nu}$ . This leaves 5 propagating modes corresponding to the physical degrees of freedom of a massive spin-two particle, the  $n$ -th Kaluza-Klein excitation of the graviton. The condition of the unitary gauge corresponds to eliminating the spin-zero ( $P^{(n)}$ ) and spin-one ( $Q^{(n)}{}_\mu$ ) particles eaten by the massless graviton to form a spin-two massive multiplet.

The fields  $V^{(n)}_{\mu j}$  (satisfying  $\hat{n}^j V^{(n)}_{\mu j} = 0$ ) describe  $\delta - 1$  spin-one particles which form massive multiplets by absorbing the fields  $P^{(n)}_j$ . These vector particles satisfy the Lorentz condition, see eq. (27), and each contains three physical degrees of freedom. They are not coupled to the energy-momentum tensor in the weak-field limit, see eq. (29), and therefore will play no role in our analysis of collider experiments. Next, for  $\delta \geq 2$ , there are  $(\delta^2 - \delta - 2)/2$  massive real scalars described by the symmetric tensor  $S^{(n)}_{jk}$ , which satisfies the relations  $\hat{n}^j S^{(n)}_{jk} = 0$ ,  $S^{(n)j}_j = 0$ . These scalars are also not coupled to matter, see eq. (30). Finally, there is the scalar  $H^{(\vec{n})}$  which is coupled only to the trace of the energy-momentum tensor, see eq. (31). If we impose the equations of motion,  $T^\mu_\mu$  vanishes for conformally-invariant theories. Thus  $H^{(\vec{n})}$  does not participate in any tree-level process involving massless matter field. The scalar  $H^{(\vec{n})}$  can only couple to ordinary particles at tree level proportionally to their masses. These couplings give effective interactions at best of order  $M_Z^2/M_D^2$ , which are negligible for our considerations. Indeed one may worry about the existence of a massless mode associated with  $H^{(\vec{n})}$ , which would lead to unwanted violations of the Equivalence Principle (a difference in Newton's constant characterizing the coupling to photons and to non-relativistic matter). The mode in question corresponds to a fluctuation, named radion in ref. [21], of the volume of the  $\delta$  compactified dimensions. Thus, whatever mechanism stabilizes the radius of the extra dimensions, it will give a mass to the radion. In ref. [21] several mechanisms of radius stabilization were described and it was shown that it is not difficult to give the radion a mass larger than  $(1 \text{ mm})^{-1} \sim 2 \times 10^{-4} \text{ eV}$ . This is sufficient to satisfy the present experimental bounds. Such a tiny mass for  $H^{(\vec{n})}$  affects our previous analysis only for the lowest Kaluza-Klein modes. As a final remark, the radion corresponds to the zero mode of  $h^j_j$ . Since  $n = 0$ , this mode cannot be gauged away even in the special case of  $\delta = 1$ , in which the radion Kaluza-Klein excitations are eaten by the massive spin-2 graviton.

Adding the numbers of physical degrees of freedom for  $G^{(n)}_{\mu\nu}$ ,  $V^{(n)}_{\mu j}$ ,  $S^{(n)}_{jk}$ , and  $H^{(\vec{n})}$  we obtain a total of  $(4 + \delta)(1 + \delta)/2$ . It is interesting to do the same counting from the point of view of the  $D$ -dimensional theory. The symmetric tensor  $h_{AB}$  contains  $D(D + 1)/2$  massless components. In order to compute the physical degrees of freedom, we first need to fix the gauge, say by the harmonic condition  $\partial_A h^A_B = \frac{1}{2} \partial_B h^A_A$  (see *e.g.* ref. [29]). Analogously to the case of QED, we then discover that, for a massless graviton, we still have residual freedom

to make gauge transformations with gauge parameters  $\epsilon_A$  subject to the condition  $\square\epsilon_A = 0$ . In total we eliminate  $2D$  components from  $h_{AB}$ , leaving  $D(D-3)/2$  physical states. For  $D = 4$  we find the 2 degrees of freedom of a massless graviton, and for  $D = 4 + \delta$  we recover the same result previously obtained from a four-dimensional Kaluza-Klein point of view.

### 3 Feynman Rules

In this section we give the Feynman rules necessary to compute the rate for graviton-emission processes. Some of the rules presented here can also be extracted from ref. [30].

We start from the  $D$ -dimensional graviton Lagrangian corresponding to the Einstein equation (6),

$$\mathcal{L} = -\frac{1}{2}h^{AB}\square h_{AB} + \frac{1}{2}h_A^A\square h_B^B - h^{AB}\partial_A\partial_B h_C^C + h^{AB}\partial_A\partial_C h_B^C - \frac{1}{\bar{M}_D^{1+\delta/2}}h^{AB}T_{AB}. \quad (42)$$

We can now follow the procedure discussed in the previous section and reduce eq. (42) into a Lagrangian describing 4-dimensional fields. We choose the field parametrization in eqs. (17)–(23) and the unitary gauge  $Q^{(n)}{}_\mu = 0$ ,  $P^{(n)}{}_j = 0$ ,  $P^{(n)} = 0$ . The meaning of this gauge choice should be clear by now. It eliminates the non-physical degrees of freedom absorbed by the massive fields, and it enables us to work with a Lagrangian with diagonal kinetic terms. In particular, notice that the shift of  $h^{(n)}{}_{\mu\nu}$  proportional to  $H^{(\bar{n})}$  in the definition of  $G^{(n)}{}_{\mu\nu}$ , eq. (17), is essential to separate the physical scalar component from the unphysical scalars contained in the 4-dimensional metric. Without this shift, the kinetic terms of the Lagrangian would mix  $H^{(\bar{n})}$  with  $G^{(n)\mu}{}_\mu$  and  $\partial^\mu\partial^\nu G^{(n)}{}_{\mu\nu}$ .

In the unitary gauge, the Lagrangian in eq. (42) becomes the sum over the Kaluza-Klein modes of

$$\begin{aligned} \mathcal{L} = & \sum_{\text{all } \bar{n}} -\frac{1}{2}G^{(-\bar{n})\mu\nu}(\square + m^2)G^{(\bar{n})}{}_{\mu\nu} + \frac{1}{2}G^{(-\bar{n})\mu}{}_\mu(\square + m^2)G^{(\bar{n})\nu}{}_\nu - G^{(-\bar{n})\mu\nu}\partial_\mu\partial_\nu G^{(\bar{n})\lambda}{}_\lambda \\ & + G^{(-\bar{n})\mu\nu}\partial_\mu\partial_\lambda G^{(\bar{n})\lambda}{}_\nu - \frac{1}{4}|\partial_\mu V^{(\bar{n})}{}_{\nu j} - \partial_\nu V^{(\bar{n})}{}_{\mu j}|^2 + \frac{m^2}{2}V^{(-\bar{n})\mu j}V^{(\bar{n})}{}_{\mu j} \\ & - \frac{1}{2}S^{(-\bar{n})jk}(\square + m^2)S^{(\bar{n})}{}_{jk} - \frac{1}{2}H^{(-\bar{n})}(\square + m^2)H^{(\bar{n})} \\ & - \frac{1}{\bar{M}_P} \left[ G^{(\bar{n})\mu\nu} - \frac{\kappa}{3}\eta^{\mu\nu}H^{(\bar{n})} \right] T_{\mu\nu}. \end{aligned}$$

Here  $m^2 \equiv \hat{n}^2$  is the Kaluza-Klein graviton squared mass and  $\kappa$  is given in eq. (24). The graviton propagator is obtained by inverting the Fourier-transformed bilinear Lagrangian in eq. (43),

$$\begin{array}{ccc} \text{---} \mathbb{G}_{\mu\nu}^{(n)}(k) & \xrightarrow{\hspace{2cm}} & \text{---} \mathbb{G}_{\alpha\beta}^{(n)}(k) & \qquad \qquad \qquad \frac{i P_{\mu\nu\alpha\beta}}{k^2 - m^2} \end{array}$$

$$\begin{aligned} P_{\mu\nu\alpha\beta} &= \frac{1}{2} (\eta_{\mu\alpha}\eta_{\nu\beta} + \eta_{\mu\beta}\eta_{\nu\alpha} - \eta_{\mu\nu}\eta_{\alpha\beta}) \\ &\quad - \frac{1}{2m^2} (\eta_{\mu\alpha}k_\nu k_\beta + \eta_{\nu\beta}k_\mu k_\alpha + \eta_{\mu\beta}k_\nu k_\alpha + \eta_{\nu\alpha}k_\mu k_\beta) \\ &\quad + \frac{1}{6} \left( \eta_{\mu\nu} + \frac{2}{m^2} k_\mu k_\nu \right) \left( \eta_{\alpha\beta} + \frac{2}{m^2} k_\alpha k_\beta \right). \end{aligned} \tag{43}$$

The spin-sum of the polarization tensors is

$$\sum_s e_{\mu\nu}(k, s) e_{\alpha\beta}(k, s) = P_{\mu\nu\alpha\beta}(k). \tag{44}$$

The tensor  $P_{\mu\nu\alpha\beta}(k)$  satisfies conditions (40)–(41), since on mass-shell

$$\eta^{\alpha\beta} P_{\mu\nu\alpha\beta}(k) = 0, \tag{45}$$

$$k^\alpha P_{\mu\nu\alpha\beta}(k) = 0. \tag{46}$$

For our considerations it is also useful to derive the massless graviton propagator in  $D$  dimensions. In order to invert the kinetic term, we need to add to the Lagrangian in eq. (42) a gauge-fixing term, which we choose to be

$$\mathcal{L} = \frac{1}{\xi} C^A C_A, \quad C_A = \partial^B h_{AB} - \frac{1}{2} \partial_A h_B^B. \tag{47}$$

Here  $\xi$  is the gauge-fixing parameter, and  $\xi = 1$  corresponds to the de Donder gauge often chosen in quantum gravity. The propagator of the massless graviton is  $iP_{ABCD}^{(0)}/k^2$ , where

$$\begin{aligned} P_{ABCD}^{(0)} &= \frac{1}{2} (\eta_{AC}\eta_{BD} + \eta_{AD}\eta_{BC}) - \frac{1}{D-2} \eta_{AB}\eta_{CD} \\ &\quad + \frac{(\xi-1)}{2k^2} (\eta_{AC}k_B k_D + \eta_{BD}k_A k_C + \eta_{AD}k_B k_C + \eta_{BC}k_A k_D). \end{aligned} \tag{48}$$

We now turn to the graviton interaction Lagrangian, which is given by

$$\mathcal{L} = -\frac{1}{M_P} G^{(n)}{}_{\mu\nu} T^{\mu\nu}. \quad (49)$$

Here  $T_{\mu\nu}$  is the energy-momentum tensor, which is symmetric and conserved. As previously discussed, the Kaluza-Klein excitations of the graviton have the same couplings to ordinary fields as their massless zero mode.

We start by discussing the case of QED coupled to quantum gravity, which is described by the Lagrangian

$$\mathcal{L} = \sqrt{-g} \left( i\bar{\psi}\gamma^a D_a \psi - \frac{1}{4} F_{\mu\nu} F^{\mu\nu} \right), \quad (50)$$

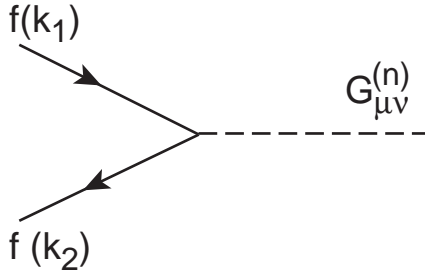
$$D_a = e_a^\mu \left( \partial_\mu - ieQ A_\mu + \frac{1}{2} \sigma^{bc} e_b^\nu \partial_\nu e_{c\mu} \right). \quad (51)$$

Here  $\sigma^{ab} = (\gamma^a \gamma^b - \gamma^b \gamma^a)/4$ ,  $e_a^\mu$  are the vierbein fields, and  $Q$  is the electric charge of the fermion  $\psi$ . Greek indices refer to general coordinate transformations and Latin indices to Lorentz transformations. By varying the Lagrangian with respect to the vierbein, we obtain

$$\begin{aligned} T_{\mu\nu} = & \frac{i}{4} \bar{\psi} (\gamma_\mu \partial_\nu + \gamma_\nu \partial_\mu) \psi - \frac{i}{4} (\partial_\mu \bar{\psi} \gamma_\nu + \partial_\nu \bar{\psi} \gamma_\mu) \psi + \\ & \frac{1}{2} eQ \bar{\psi} (\gamma_\mu A_\nu + \gamma_\nu A_\mu) \psi + F_{\mu\lambda} F^\lambda{}_\nu + \frac{1}{4} \eta_{\mu\nu} F^{\lambda\rho} F_{\lambda\rho}. \end{aligned} \quad (52)$$

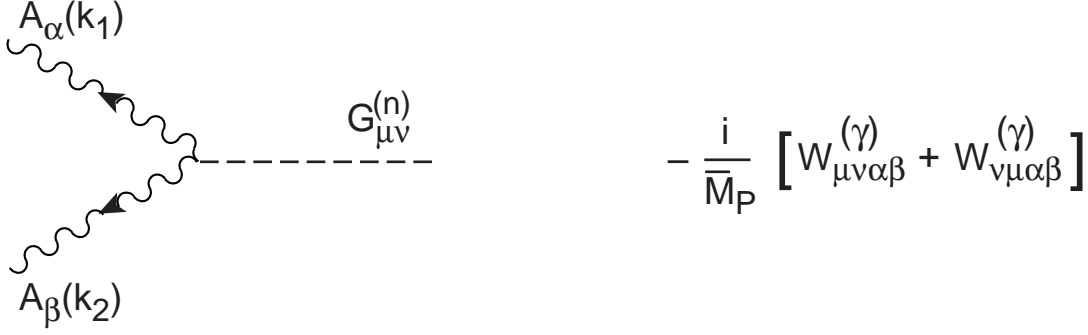
Notice that the trace of the above energy-momentum tensor is zero on the equations of motion, as a result of the tree-level conformal invariance of a massless gauge theory.

From eq. (49), we obtain the following Feynman rules:



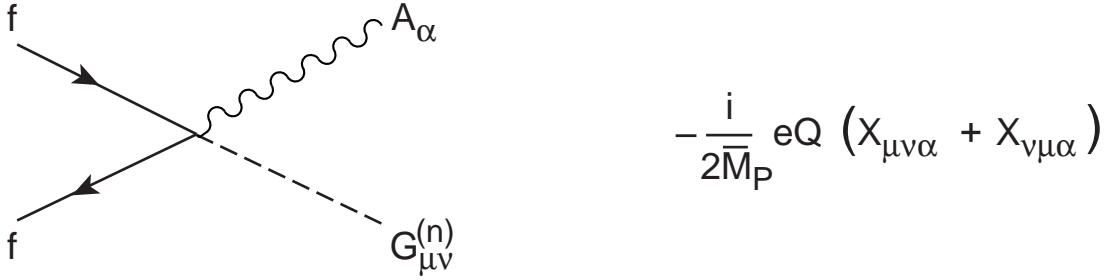
$$-\frac{i}{4M_P} \left[ W_{\mu\nu}^{(f)} + W_{\nu\mu}^{(f)} \right]$$

$$W_{\mu\nu}^{(f)} = (k_1 + k_2)_\mu \gamma_\nu \quad (53)$$



$$-\frac{i}{\bar{M}_P} \left[ W_{\mu\nu\alpha\beta}^{(\gamma)} + W_{\nu\mu\alpha\beta}^{(\gamma)} \right]$$

$$W_{\mu\nu\alpha\beta}^{(\gamma)} = \frac{1}{2} \eta_{\mu\nu} (k_{1\beta} k_{2\alpha} - k_1 \cdot k_2 \eta_{\alpha\beta}) + \eta_{\alpha\beta} k_{1\mu} k_{2\nu} + \eta_{\mu\alpha} (k_1 \cdot k_2 \eta_{\nu\beta} - k_{1\beta} k_{2\nu}) - \eta_{\mu\beta} k_{1\nu} k_{2\alpha} \quad (54)$$

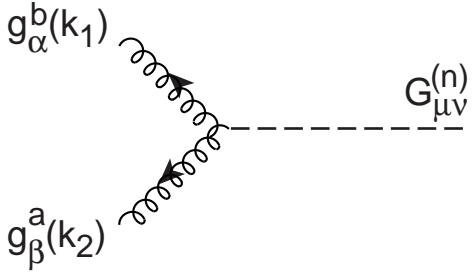


$$-\frac{i}{2\bar{M}_P} eQ (X_{\mu\nu\alpha} + X_{\nu\mu\alpha})$$

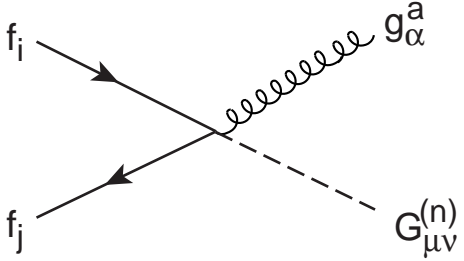
$$X_{\mu\nu\alpha} = \gamma_\mu \eta_{\nu\alpha}. \quad (55)$$

We follow the convention that particle momenta (indicated inside parenthesis when necessary) flow along the arrow directions.

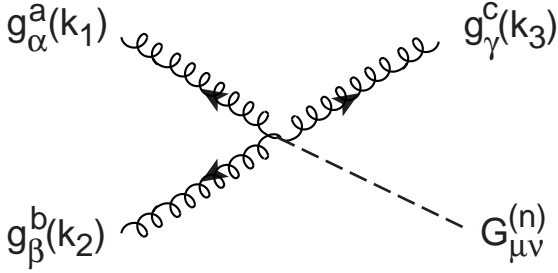
The generalization of these results to the case of QCD coupled to quantum gravity is straightforward. The energy-momentum tensor for QCD has the same form as eq. (52) with the replacements  $eQA_\mu \rightarrow g_s A_\mu^a t^a$ ,  $F_{\mu\nu} \rightarrow G_{\mu\nu}^a = \partial_\mu A_\nu^a - \partial_\nu A_\mu^a - g_s f^{abc} A_\mu^b A_\nu^c$ , where  $a, b, c$  are group indices,  $t^a$  are group generators in the fundamental representation, and  $f^{abc}$  are the structure constants. We then obtain the following Feynman rules:



$$-\frac{i}{\overline{M}_P} \delta^{ab} \left[ W_{\mu\nu\alpha\beta}^{(\gamma)} + W_{\nu\mu\alpha\beta}^{(\gamma)} \right]$$



$$-\frac{i}{2\overline{M}_P} g_s t_{ji}^a (X_{\mu\nu\alpha} + X_{\nu\mu\alpha})$$



$$\frac{g_s}{\overline{M}_P} f^{abc} \left[ Y(k_1)_{\mu\nu\alpha\beta\gamma} + Y(k_2)_{\mu\nu\beta\gamma\alpha} + Y(k_3)_{\mu\nu\gamma\alpha\beta} \right. \\ \left. + Y(k_1)_{\nu\mu\alpha\beta\gamma} + Y(k_2)_{\nu\mu\beta\gamma\alpha} + Y(k_3)_{\nu\mu\gamma\alpha\beta} \right]$$

$$Y(k) = k_\mu (\eta_{\nu\beta}\eta_{\alpha\gamma} - \eta_{\nu\gamma}\eta_{\alpha\beta}) \\ + k_\beta \left( \eta_{\mu\alpha}\eta_{\nu\gamma} - \frac{1}{2}\eta_{\mu\nu}\eta_{\alpha\gamma} \right) - k_\gamma \left( \eta_{\mu\alpha}\eta_{\nu\beta} - \frac{1}{2}\eta_{\mu\nu}\eta_{\alpha\beta} \right). \quad (56)$$

Since we will not make use of the vertex with four gluons and a graviton, we will not write it down explicitly.

## 4 Graviton Production Processes

We now consider the physical processes relevant to collider experiments, starting with graviton production. The graviton Kaluza-Klein modes have masses equal to  $|n|/R$ , and therefore

the different excitations have mass splittings

$$\Delta m \sim \frac{1}{R} = M_D \left( \frac{M_D}{\bar{M}_P} \right)^{2/\delta} \sim \left( \frac{M_D}{\text{TeV}} \right)^{\frac{\delta+2}{2}} 10^{\frac{12\delta-31}{\delta}} \text{eV}. \quad (57)$$

Here we have used the relation between the compactification radius  $R$  and the effective Planck mass of the  $D$ -dimensional theory  $M_D$ , eq. (16). If we take  $M_D = 1$  TeV and  $\delta = 4, 6, 8$ , then  $\Delta m$  is equal to 20 keV, 7 MeV, and 0.1 GeV, respectively. Only for a large number of extra dimensions does the mass splitting become comparable with the experimental energy resolution. However, for large  $\delta$ , only a small number of Kaluza-Klein modes can be produced and the total cross-section is negligible. We are interested in the case in which  $\delta$  is not too large (say  $\delta \lesssim 6$ ), where the enormous number of accessible Kaluza-Klein modes can compensate the  $1/\bar{M}_P^2$  factor in the scattering amplitude.

For experimental applications, it is convenient to express the graviton-production rate in terms of inclusive cross-sections, where the contributions of the different Kaluza-Klein modes have been summed up. For not too large  $\delta$ , the mass splitting  $\Delta m$  is so small that the sum over the different Kaluza-Klein states can be replaced by a continuous integration. The number of modes with Kaluza-Klein index between  $|n|$  and  $|n| + dn$  is given by

$$dN = S_{\delta-1} |n|^{\delta-1} dn, \quad S_{\delta-1} = \frac{2\pi^{\delta/2}}{\Gamma(\delta/2)}, \quad (58)$$

where  $S_{\delta-1}$  is the surface of a unit-radius sphere in  $\delta$  dimensions<sup>§</sup>. Using eq. (16) and the expression  $m = |n|/R$  for the Kaluza-Klein excitation mass, we can rewrite the measure in eq. (58) as

$$dN = S_{\delta-1} \frac{\bar{M}_P^2}{M_D^{2+\delta}} m^{\delta-1} dm. \quad (59)$$

Hence we express the differential cross-section for inclusive graviton production as

$$\frac{d^2\sigma}{dt dm} = S_{\delta-1} \frac{\bar{M}_P^2}{M_D^{2+\delta}} m^{\delta-1} \frac{d\sigma_m}{dt}, \quad (60)$$

where  $d\sigma_m/dt$  is the differential cross-section for producing a single Kaluza-Klein graviton of mass  $m$ . Since the graviton interaction vertex is suppressed by  $1/\bar{M}_P$  (see sect. 3) we can

---

<sup>§</sup>For  $\delta = 2n$  and  $n$  integer, we find  $S_{\delta-1} = 2\pi^n/(n-1)!$  and, for  $\delta = 2n+1$ , we find  $S_{\delta-1} = 2\pi^n/\prod_{k=0}^{n-1}(k + \frac{1}{2})$ .

anticipate that  $\sigma_m \propto \bar{M}_P^{-2}$ , and the factor  $\bar{M}_P^2$  appearing from the phase-space summation exactly cancels the Planck mass dependence in eq. (60).

The same result can also be obtained from the point of view of the  $D$ -dimensional theory. Here, the canonically normalized graviton  $h_{AB}$  has a coupling to matter  $\mathcal{L}_D = -T^{AB}h_{AB}/\bar{M}_D^{1+\delta/2}$ . The graviton phase space is

$$d\Phi_G = \frac{d^{D-1}k_D}{(2\pi)^{D-1}2\sqrt{k_D \cdot k_D}} = \frac{d^\delta k_T}{(2\pi)^\delta} \times \frac{d^3k}{(2\pi)^3 2\sqrt{\vec{k}^2 + m^2}}, \quad (61)$$

where we have decomposed  $k_D$  in the components  $k_T$  and  $k$  respectively orthogonal and parallel to the brane. Graviton emission from the brane is, in lowest order, independent of the orientation of  $k_T$  so we can trivially integrate on it:  $d^\delta k_T = S_{\delta-1}m^{\delta-1}dm$ . The cross section for an initial brane state  $|p_1, p_2\rangle$  to go in a final brane state  $|f\rangle$  plus a bulk graviton  $|G\rangle$  is then

$$d\sigma = \frac{S_{\delta-1}m^{\delta-1}dm}{\bar{M}_D^{2+\delta}} |\langle f, G | T^{\mu\nu} h_{\mu\nu} | p_1, p_2 \rangle|^2 (2\pi)^4 \delta^4(P_i - P_f) \frac{d\Phi_f}{F(p_1, p_2)}, \quad (62)$$

where  $d\Phi_f$  is the brane final state phase space, and  $F(p_1, p_2)$  is just the usual flux factor for two particle collision. This equation agrees with eq. (60).

We now give the differential cross-sections for producing a Kaluza-Klein graviton of mass  $m$  in processes which are relevant to the high-energy collider experiments discussed in the sect. 6. The cross-section for producing a graviton and a photon in a fermion-antifermion collision is

$$\frac{d\sigma_m}{dt}(f\bar{f} \rightarrow \gamma G) = \frac{\alpha Q_f^2}{16N_f} \frac{1}{s\bar{M}_P^2} F_1(t/s, m^2/s). \quad (63)$$

Here  $Q_f$  and  $N_f$  are the electric charge and number of colours of the fermion  $f$ , and  $F_1$  is provided in the appendix. The cross-sections for the parton processes relevant to graviton plus jet production in hadron collisions are

$$\frac{d\sigma_m}{dt}(q\bar{q} \rightarrow gG) = \frac{\alpha_s}{36} \frac{1}{s\bar{M}_P^2} F_1(t/s, m^2/s) \quad (64)$$

$$\frac{d\sigma_m}{dt}(qg \rightarrow qG) = \frac{\alpha_s}{96} \frac{1}{s\bar{M}_P^2} F_2(t/s, m^2/s) \quad (65)$$

$$\frac{d\sigma_m}{dt}(gg \rightarrow gG) = \frac{3\alpha_s}{16} \frac{1}{sM_P^2} F_3(t/s, m^2/s) \quad (66)$$

The Mandelstam variable  $t$  in eq. (65) is defined as  $t = (p_q - p_G)^2$ . The functions  $F_2$  and  $F_3$  are provided in the appendix.

We want to stress again that our calculation of graviton emission is based on an effective low-energy theory, valid below the scale  $M_D$ . Of course, we cannot determine the precise scale at which our effective low-energy theory breaks down. Nevertheless, we can use naive dimensional analysis to estimate the energy scale at which perturbation theory breaks down. If we analyse graviton loop corrections in  $D$  dimensions, we observe that the expansion parameter is [31]

$$\frac{S_{D-1}}{2(2\pi)^D} \left( \frac{E}{M_D} \right)^{D-2}. \quad (67)$$

Here,  $S_{D-1}$  is the surface of the  $D$ -sphere given in eq. (58), and  $E$  is the relevant energy of the process. Requiring that the expansion parameter is less than unity, we obtain an estimate of the maximum energy at which we can trust a perturbative expansion in the effective theory

$$E_{\max} = [\Gamma(2 + \delta/2)]^{\frac{1}{2+\delta}} (4\pi)^{\frac{4+\delta}{4+2\delta}} M_D. \quad (68)$$

Numerically, one finds always that  $E_{\max} > 7.2M_D$ . Although perturbativity can be trusted up to  $E_{\max}$ , new quantum-gravity effects may appear much sooner, as mentioned in the introduction.

## 5 Virtual Graviton Exchange

We now want to study the effect of a single virtual-graviton exchange at tree-level in scattering processes. For simplicity we consider the case of pure  $s$ -channel exchange, but the discussion of the  $t$ - and  $u$ -channel exchange is completely analogous. The scattering amplitude in momentum space of the graviton-mediated process is

$$\mathcal{A} = \frac{1}{M_P^2} \sum_n \left[ T_{\mu\nu} \frac{P^{\mu\nu\alpha\beta}}{s - m^2} T_{\alpha\beta} + \left( \frac{\kappa}{3} \right)^2 \frac{T_\mu^\mu T_\nu^\nu}{s - m^2} \right] = \mathcal{S}(s) \mathcal{T} \quad (69)$$

$$\mathcal{S}(s) \equiv \frac{1}{M_P^2} \sum_n \frac{1}{s - m^2} \quad (70)$$

$$\mathcal{T} \equiv T_{\mu\nu}T^{\mu\nu} - \frac{1}{\delta+2}T_{\mu}^{\mu}T_{\nu}^{\nu}. \quad (71)$$

Here  $T_{\mu\nu}$  is the energy-momentum tensor,  $k$  is the transferred momentum,  $\kappa$  is defined in eq. (24), and  $P^{\mu\nu\alpha\beta}$  in eq. (43). The two terms in eq. (69) correspond to the exchange of the graviton  $G^{(n)}_{\mu\nu}$  and the scalar  $H^{(\vec{n})}$ . The same result can be obtained by exchanging a massless  $D$ -dimensional graviton with the propagator in eq. (49) and with coupling to the energy-momentum tensor given in eq. (11). In eq. (69)  $\sum_n$  represents the sum over all Kaluza-Klein modes, which has to be performed at the amplitude level. Since the operator  $\mathcal{T}$  does not depend on the Kaluza-Klein index, we can perform the sum  $\sum_n$  without specifying the particular physical scattering process under consideration. It is convenient to convert the sum into an integral which can be evaluated using dimensional regularization:

$$\mathcal{S}(s) = \frac{1}{M_D^{2+\delta}} \int d^\delta q_T \frac{1}{s - q_T^2} = \pi^{\frac{\delta}{2}} \Gamma(1 - \delta/2) \left( -\frac{s}{M_D^2} \right)^{\frac{\delta}{2}-1}. \quad (72)$$

Here we used  $m^2 = q_T^2$ , with  $q_T$  the graviton momentum orthogonal to the brane. To further simplify eq. (72), we need to distinguish the cases in which  $\delta$  is even or odd. For even  $\delta$  ( $\delta \geq 4$ ), we find

$$\mathcal{S}(s) = -\frac{1}{M_D^{2+\delta}} \frac{S_{\delta-1}}{2} \left[ \left( i\pi + \ln \frac{s}{\mu^2} \right) s^{\frac{\delta-2}{2}} + \sum_{k=1}^{(\delta-2)/2} c_k \Lambda^{\delta-2k} s^{k-1} \right] \quad (73)$$

and for odd  $\delta$  ( $\delta \geq 3$ ),

$$\mathcal{S}(s) = -\frac{1}{M_D^{2+\delta}} \frac{S_{\delta-1}}{2} \left[ i\pi \sqrt{s} s^{\frac{\delta-3}{2}} + \sum_{k=1}^{(\delta-1)/2} c_k \Lambda^{\delta-2k} s^{k-1} \right]. \quad (74)$$

Here  $S_{\delta-1}$  is defined in eq. (58),  $\mu$  is the subtraction mass,  $\Lambda$  is an ultraviolet cutoff, and  $c_k$  are unknown coefficients. The terms proportional to  $\Lambda$  describe divergent terms not computable in the effective theory. The presence of ultraviolet divergences in tree-level processes is related to existence of an infinite tower of Kaluza-Klein modes. In the case  $\delta = 2$ , there are no power divergences and  $\mathcal{S}(s)$  is given by eq. (73) with the summation over  $k$  omitted.

The non-analytic pieces proportional to  $\ln(-s)$  and  $\sqrt{-s}$  in  $\mathcal{S}(s)$  are determined by low-energy physics only. This is because they have branch-cut singularities – the imaginary parts in eqs. (73), (74) – corresponding to real graviton emission. Therefore this dependence is

uniquely fixed as it cannot be affected by the introduction of local counterterms [31]. Notice that these effects are the analogue of the familiar “running” of amplitudes in quantum field theory, although here we are apparently dealing with a tree-level calculation.

Unfortunately,  $\mathcal{S}(s)$  is dominated by the ultraviolet contributions, which can be computed only with some knowledge of the underlying quantum-gravity theory. The infrared contributions could be experimentally isolated only if the coefficients  $c_k$  turn out to be small (because of some “miraculous” cancellation of divergences in the fundamental theory), or with very precise measurements of the energy dependence or angular dependence (in case of  $t$ -channel graviton exchange) of the scattering process. The case  $\delta = 2$  is particularly interesting, since there is only a logarithmic dependence on the cutoff. However, for phenomenological applications, we will adopt the most plausible assumption that  $\mathcal{S}(s)$  is dominated by the lowest-dimensional local operator, and that the amplitude of the physical process is described by

$$\mathcal{A} = \frac{S_{\delta-1}}{2} c_1 \frac{\Lambda^{\delta-2}}{M_D^{\delta+2}} \mathcal{T} \equiv \frac{4\pi}{\Lambda_T^4} \mathcal{T} \quad \text{for } \delta > 2. \quad (75)$$

Here  $\Lambda$  is the unknown cutoff energy, presumably of order  $M_D$ . In the case of string theory, the effective cutoff could appear at a scale lower than  $M_D$ , giving a suppression of the amplitude.

From eq. (75), we can compute the cross-sections for various processes relevant to collider experiments. For instance, the cross-sections for processes with two photons in the final state are

$$\frac{d\sigma}{dt}(f\bar{f} \rightarrow \gamma\gamma) = \frac{2\pi}{N_f s^2} \left[ \alpha Q_f^2 G_1(t/s) + \frac{2s^2}{\Lambda_T^4} G_2(t/s) \right]^2 \quad (76)$$

$$\frac{d\sigma}{dt}(gg \rightarrow \gamma\gamma) = \frac{\pi}{16} \frac{s^2}{\Lambda_T^8} G_3(t/s), \quad (77)$$

and the cross-section for the fermion scattering process  $e^+e^- \rightarrow f\bar{f}$  (with  $f \neq \nu_e$ ) is

$$\begin{aligned} \frac{d\sigma}{dt}(e^+e^- \rightarrow f\bar{f}) &= \frac{d\sigma}{dt}(e^+e^- \rightarrow f\bar{f})_{\text{SM}} + \frac{N_f \pi}{32} \frac{s^2}{\Lambda_T^8} G_4(t/s) \\ &- \frac{N_f \alpha \pi}{2\Lambda_T^4} \left\{ Q_e Q_f G_5(t/s) + \frac{1}{\sin^2 2\theta_W} \frac{s}{s - M_Z^2} [v_e v_f G_5(t/s) + a_e a_f G_6(t/s)] \right\} \\ &- \frac{\alpha \pi}{2\Lambda_T^4} \delta_{ef} \left\{ Q_e^2 G_7(t/s) + \frac{s}{\sin^2 2\theta_W} \frac{v_e^2 + a_e^2}{s - M_Z^2} G_8(t/s) \right\} \end{aligned}$$

$$+ \frac{1}{\sin^2 2\theta_W} \frac{s}{t - M_Z^2} \left[ v_e^2 G_9(t/s) + a_e^2 G_{10}(t/s) \right] \Big\} + \frac{\delta_{ef}\pi}{32} \frac{s^2}{\Lambda_T^8} G_{11}(t/s), \quad (78)$$

where  $v_f = T_f - 2Q_f \sin^2 \theta_W$ ,  $a_f = T_f$  and  $t = (p_{e^-} - p_f)^2$ . The symbol  $\delta_{ef}$  is equal to 1 if the final-state fermion is an electron ( $f = e$ ), and is equal to 0 otherwise. The  $G_i(x)$  functions are given in the appendix. Collider tests of the existence of the operator  $\mathcal{T}$  will be discussed in sect. 7, where we study the  $f\bar{f} \rightarrow \gamma\gamma$  case as an example.

Before concluding this section, we use eqs. (73)–(74) to derive a limit on the applicability of the effective theory from unitarity arguments. Using the Wigner-Eckart theorem, we can decompose the transition amplitude between an initial state  $i$  and a final state  $f$  into helicity amplitudes

$$\mathcal{A}_{fi} = 8\pi \sum_J (2J + 1) \mathcal{D}_{fi}^J(\theta) \langle f | T^J | i \rangle. \quad (79)$$

Here  $\mathcal{D}$  are the Wigner functions which depend on the scattering angle  $\theta$ . Let us now consider the scattering process between two pairs of different fermions  $f\bar{f} \rightarrow G \rightarrow f'\bar{f}'$ , mediated by graviton exchange in the  $s$ -channel. For an initial and final state of helicity one, we obtain

$$\langle f_{\lambda=1} | T^{J=2} | i_{\lambda=1} \rangle = \frac{s^2}{160\pi} \mathcal{S}(s). \quad (80)$$

By unitarity it must be  $|T_{fi}^{J=2}| < 1$ , and in particular  $|\text{Im}T_{fi}^{J=2}| < 1$ . Therefore, using eqs. (73) and (74), we find that unitarity is violated unless

$$\sqrt{s} < \left[ 160\pi^{-\delta/2} \Gamma(\delta/2) \right]^{\frac{1}{2+\delta}} M_D. \quad (81)$$

Here,  $\sqrt{s_{\text{max}}}/M_D$  is greater than 1.4 for  $\delta \leq 5$ .

## 6 Graviton Production and Collider Experiments

We will now discuss the possibility of studying graviton production at high-energy colliders. Gravitons couple to matter only gravitationally, but the  $1/\bar{M}_P^2$  suppression present in their production cross-section can be compensated by the large multiplicity of the Kaluza-Klein modes or, in other words, by the  $D$ -dimensional phase-space factor. However the  $1/\bar{M}_P^2$  suppression in the graviton decay rate into ordinary matter is not compensated by phase space and therefore its lifetime is  $\tau_G \sim \bar{M}_P^2/m^3 \sim (\text{TeV}/m)^3 10^3$  seconds. The  $1/\bar{M}_P^2$

suppression factor can be also interpreted as the small probability that a graviton propagating in the  $D$ -dimensional space crosses the 3-dimensional brane.

For experimental purposes, this means that the Kaluza-Klein graviton behaves like a massive, non-interacting, stable particle and its collider signature is imbalance in final state momenta and missing mass. Since the relevant observables for graviton production are described only by inclusive cross-sections, the graviton has a continuous distribution in mass, described by eq. (60). This mass distribution corresponds to the probability of emitting gravitons with different momenta in the extra dimensions. Notice that this is a peculiarity of the graviton signal with respect to other new-physics processes. For instance, supersymmetry with conserved R-parity also can yield an excess of missing energy events, but these correspond to a fixed invisible-particle mass. Signals with topologies similar to those discussed in the following can also be encountered in phenomenological scenarios with ultralight gravitinos [32]. At any rate, graviton production leads to energy and angular distributions that are in general distinct from those corresponding to other new-physics processes. Moreover, in the case of supersymmetry, the missing-energy signal is always accompanied by a variety of leptons, photons, and hadronic activity coming from the decay of heavier particles. For graviton-production in the perturbative regime, each extra particle in the final state is associated with an extra suppression factor.

The emission of a single graviton in the extra dimensions violates momentum conservation along the directions transverse to the brane. This is not surprising, since translational invariance in the  $D$ -dimensional space is broken by the presence of the brane. In other words, the brane can radiate gravitons into the extra dimensions conserving the total energy (since time invariance is preserved), but absorbing any arbitrary transverse momentum smaller than the energy tension. From a 4-dimensional point of view, energy and momentum are conserved, but the Kaluza-Klein gravitons can have any arbitrary mass smaller than about  $M_D$ , the approximate cutoff on the validity of our description.

## 6.1 $e^+e^-$ and Muon Colliders

We start our analysis by studying future high-energy  $e^+e^-$  and  $\mu^+\mu^-$  colliders. Since both cases require an analogous discussion, for simplicity we will just refer to  $e^+e^-$  collisions. We

will focus on the graviton-production process  $e^+e^- \rightarrow \gamma G$ , but similar considerations hold for  $e^+e^- \rightarrow ZG$ . Using eqs. (60) and (63), the corresponding differential cross-section is

$$\frac{d^2\sigma}{dx_\gamma d\cos\theta}(e^+e^- \rightarrow \gamma G) = \frac{\alpha}{64} S_{\delta-1} \left(\frac{\sqrt{s}}{M_D}\right)^{\delta+2} \frac{1}{s} f(x_\gamma, \cos\theta) \quad (82)$$

$$\begin{aligned} f(x, y) &= x(1-x)^{\frac{\delta}{2}-1} F_1\left(-\frac{x}{2}(1-y), 1-x\right) \\ &= \frac{2(1-x)^{\frac{\delta}{2}-1}}{x(1-y^2)} \left[(2-x)^2(1-x+x^2) - 3y^2x^2(1-x) - y^4x^4\right]. \end{aligned} \quad (83)$$

Here  $x_\gamma = 2E_\gamma/\sqrt{s}$ ,  $E_\gamma$  is the photon energy, and  $\theta$  is the angle between the photon and beam directions. Although we are considering a two-body process, the differential cross-section depends on two kinematic variables, because of the continuous distribution in the graviton mass  $m = \sqrt{s(1-x_\gamma)}$ . The differential cross-section in eq. (82) diverges as  $x_\gamma \rightarrow 0$  or  $\cos^2\theta \rightarrow 1$ . This is caused by the collinear divergence originating from the massless fermion exchange in the  $t$  channel. Notice that, for  $\delta > 2$ , the factor  $(1-x)^{\frac{\delta}{2}-1}$  in eq. (83) tilts the photon energy spectrum towards small values of  $E_\gamma$ . The origin of this effect is the much wider graviton phase space available at large values of  $m$  (see eq. (60)).

The Standard Model background comes predominantly from the process  $e^+e^- \rightarrow \gamma\nu\bar{\nu}$ . The peak contribution from  $e^+e^- \rightarrow \gamma Z$  can be eliminated by excluding the photon-energy region around  $E_\gamma = (s - M_Z^2)/(2\sqrt{s})$ . On the other hand, the remaining continuous distribution in  $E_\gamma$  from  $e^+e^- \rightarrow \gamma\nu\bar{\nu}$  represents a significant background. Other background contributions, *e.g.* from  $e^+e^- \rightarrow \gamma(e^+e^-)$  or  $e^+e^- \rightarrow \gamma(\gamma)$ , are not important in the region of large photon transverse energy we will consider below.

In fig. 1 we show the total cross-section for  $E_{T,\gamma} \equiv E_\gamma \sin\theta > E_{T,\gamma}^{\min}$  and  $E_\gamma < 450$  GeV at a hypothetical future collider with  $\sqrt{s} = 1$  TeV. The signal is plotted for a value of the  $D$ -dimensional Planck scale  $M_D = 1.5$  TeV, and different numbers of extra dimensions  $\delta$ . The cut in  $E_\gamma$  is chosen to exclude the background contribution from the  $Z$  peak. The background shown in fig. 1 has been computed using the program COMPHEP [33]. Since the signal has been calculated at the leading order, for consistency the background is computed with the same approximation. Nevertheless, we have compared the background calculation

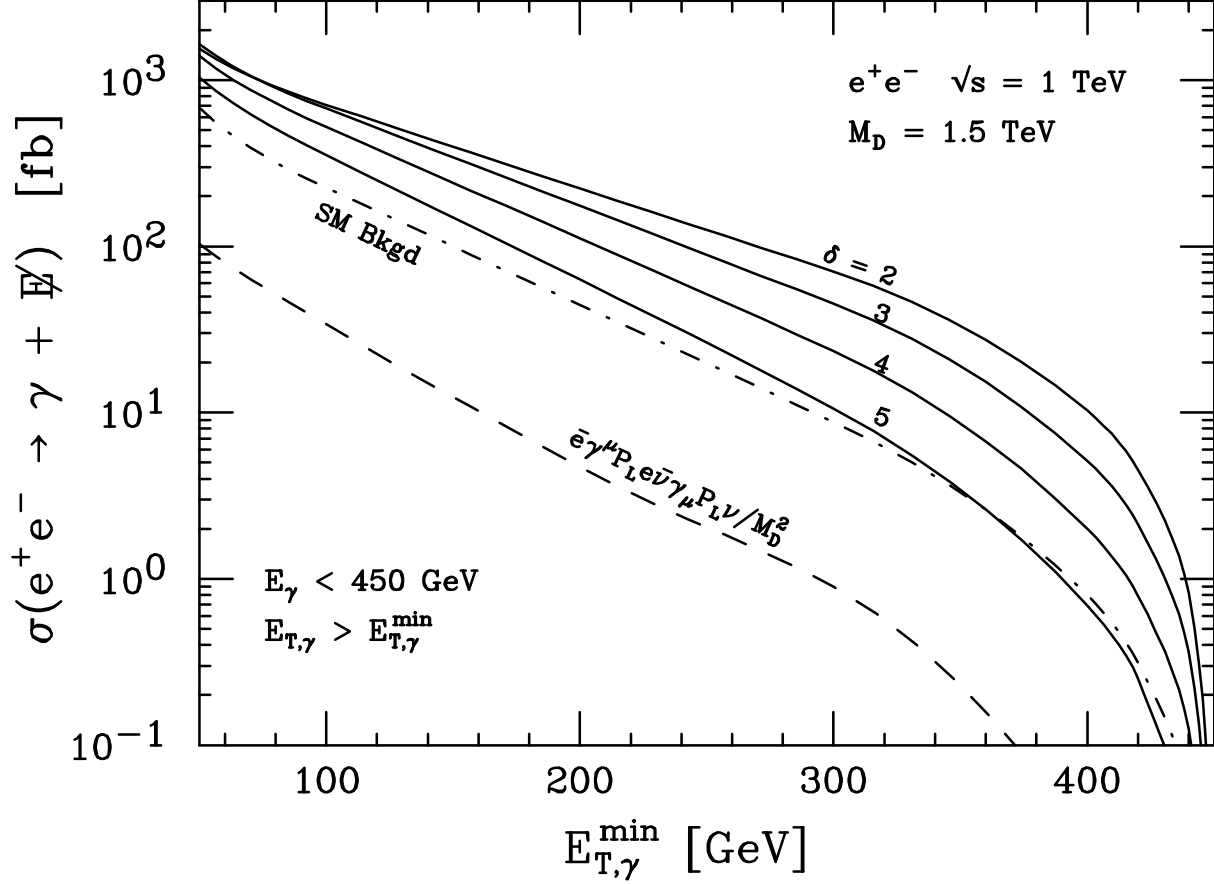


Figure 1: Total  $\gamma + \text{nothing}$  cross-section at an  $e^+e^-$  collider for  $\sqrt{s} = 1 \text{ TeV}$  with  $E_{T,\gamma} > E_{T,\gamma}^{\min}$ . The dash-dotted line represents the background, and the solid lines represent the signal for various numbers of extra dimensions and  $M_D = 1.5 \text{ TeV}$ . To eliminate the background contribution from  $\gamma Z \rightarrow \gamma \bar{\nu}\nu$  we have required  $E_\gamma < 450 \text{ GeV}$  for both the signal and the background. The dashed line is the Standard Model background subtracted signal from a representative dimension-6 operator.

to NUNUGPV [34], which includes higher order QED radiative corrections, and found agreement to within 10% at this energy.

Notice that signal and background rates have rather similar behaviours with  $E_{T,\gamma}^{\min}$ . This is because the enhanced sphericity of the signal with respect to the background is compensated by the phase-space preference to produce heavier Kaluza-Klein gravitons and therefore softer photons. The tendency towards heavier gravitons grows with  $\delta$  (see eq. (60)), as apparent from the steeper decrease of the curves with larger  $\delta$  in fig. 1.

Next we fix  $E_{T,\gamma}^{\min} = 300$  GeV and show in fig. 2 the signal rate as a function of  $M_D$ , and compare it to the Standard Model background. The dependence of the cross-section on  $M_D$  is just given by the scaling relation  $\sigma \propto 1/M_D^{2+\delta}$ . To extract the range of  $M_D$  which can be probed at a future  $e^+e^-$  collider with  $\sqrt{s} = 1$  TeV and an integrated luminosity  $\mathcal{L} = 200$  fb $^{-1}$ , we require

$$\sigma_{\text{Signal}} > \frac{5\sqrt{\sigma_{\text{Bkgd}}\mathcal{L}}}{\mathcal{L}} = 1.0 \text{ fb.} \quad (84)$$

The results for the corresponding maximum values of  $M_D$  are given in table 1. We want to stress that we have not tried to optimize our cuts, and therefore our results are just indicative of the possibilities. Dedicated analyses including higher-order corrections, improved cut choices, and detector simulations are not within the scope of this paper, although they would certainly increase the region of predicted discovery reach in  $M_D$ . Notice that the sensitivity range of  $M_D$  for colliders with different centre-of-mass energies can be obtained simply by rescaling fig. 2, since the variable  $M_D$  always appears in the cross-section in the combination  $M_D/\sqrt{s}$ .

Stringent bounds on  $M_D$  come from the requirement that graviton emission does not rapidly cool SN1987A, preventing the occurrence of the observed neutrino flux. This bound has been estimated in ref. [1] to be about  $M_D \gtrsim 10^{\frac{15-4.5\delta}{\delta+2}}$  TeV, *i.e.* 30 TeV for  $\delta = 2$  and 2 TeV for  $\delta = 3$ . Therefore, the astrophysical argument excludes observable signals for  $\delta = 2$ , limits the available region for  $\delta = 3$ , and is insignificant for  $\delta > 3$ . Nevertheless, even for  $\delta = 2$ , it is still interesting to have an independent laboratory test.

The ability to observe the signal is limited by the background which, with our cut on  $E_\gamma < 450$  GeV, is primarily coming from processes involving virtual  $W$  exchange. Therefore, with the use of polarized beams, the background can be significantly reduced without affecting

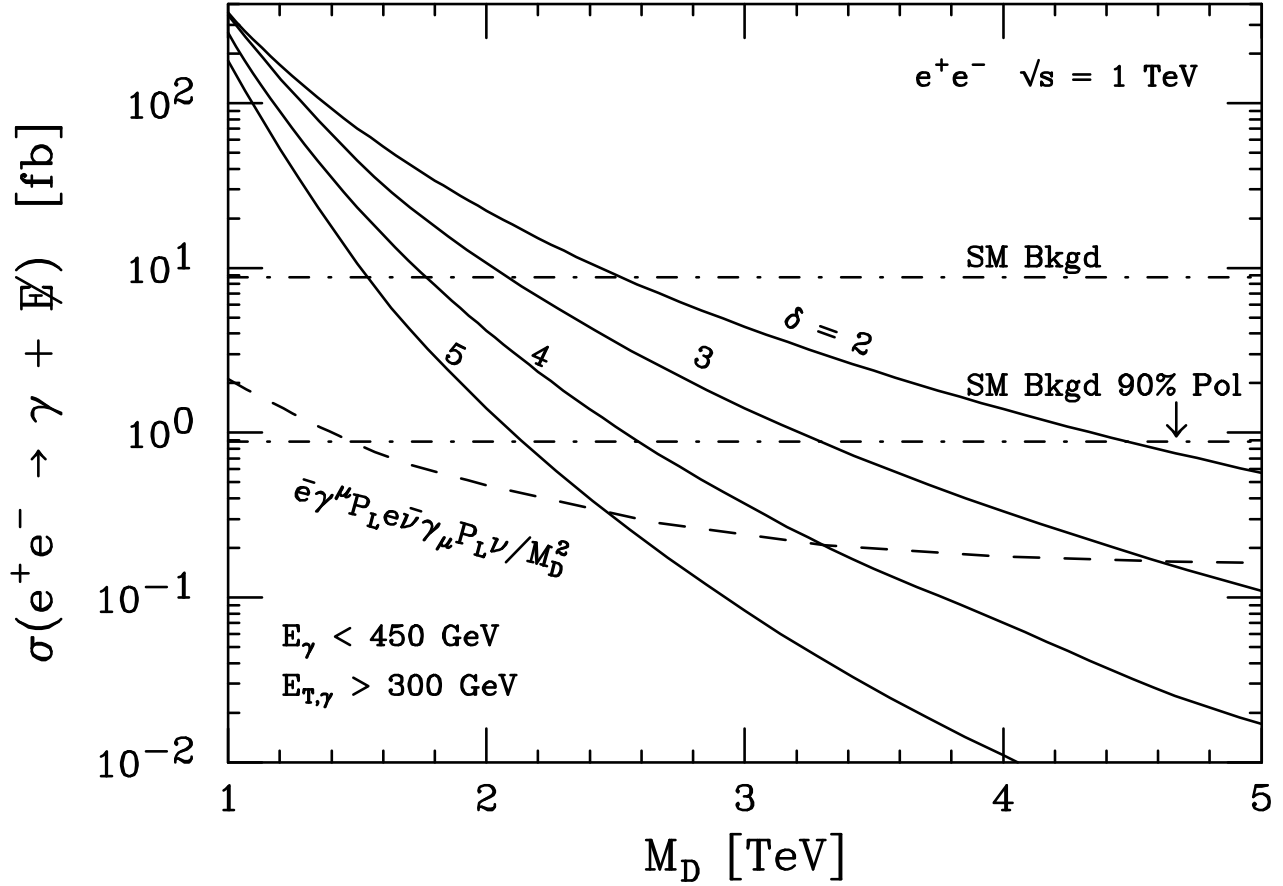


Figure 2: Total  $e^+e^- \rightarrow \gamma + \text{nothing}$  cross-section at a 1 TeV centre-of-mass energy  $e^+e^-$  collider. The signal from graviton production is presented as solid lines for various numbers of extra dimension ( $\delta = 2, 3, 4, 5$ ). The Standard Model background for unpolarized beams is given by the upper dash-dotted line, and the background with 90% polarization is given by the lower dash-dotted line. The signal and background are computed with the requirement  $E_\gamma < 450 \text{ GeV}$  in order to eliminate the  $\gamma Z \rightarrow \gamma \bar{\nu} \nu$  contribution to the background. The dashed line is the Standard Model background subtracted signal from a representative dimension-6 operator.

$\delta$	Max $M_D$ sensitivity $P = 0\%$	Max $M_D$ sensitivity $P = 90\%$
2	4.1 TeV	5.7 TeV
3	3.1	4.0
4	2.5	3.0
5	2.0	2.4

Table 1: Maximum  $M_D$  sensitivity which can be reached by studying the final state  $\gamma + \cancel{E}$  at an  $e^+e^-$  collider with  $\sqrt{s} = 1$  TeV, integrated luminosity  $\mathcal{L} = 200 \text{ fb}^{-1}$ , and beam polarization  $P = 0\%$  or  $90\%$ . The bounds have been obtained by requiring  $\sigma_{\text{Signal}} > 1.0 \text{ fb}$  with the acceptance cuts  $E_\gamma < 450 \text{ GeV}$  and  $E_{T,\gamma} > 300 \text{ GeV}$ .

the signal, which is parity invariant. In fig. 2 and table 1 we show the effect of considering collisions between an unpolarized positron beam with an electron beam with polarization  $P = 90\%$  ( $P = 100\%$  for fully right-handed electrons).

In contrast with the case of  $e^+e^-$  colliders, in muon colliders it appears arduous to obtain significant polarizations. However, a peculiarity of the muon collider is the possibility of very precise beam-energy resolution, due to small initial-state radiation and bremsstrahlung. This is useful in the search for graviton emission, since it allows precise measurements of the rapid rise of the cross-section with  $\sqrt{s}$ . Such measurements give direct information on the number of extra dimensions  $\delta$  and on the onset of quantum gravity.

Limits on  $M_D$  can be obtained from LEP2 as well. To estimate the sensitivity to  $M_D$ , we calculate the background and signal integrated over

$$10 \text{ GeV} < E_\gamma < (s - M_Z^2)/(2\sqrt{s}) - 5 \text{ GeV} \quad \text{and} \quad \theta_\gamma > 10^\circ. \quad (85)$$

The upper-limit cut on  $E_\gamma$  is intended to reduce the  $\gamma Z \rightarrow \gamma \bar{\nu} \nu$  background. The  $\gamma \bar{\nu} \nu$  cross-section with initial state radiative corrections is known to be almost a factor of two larger than the tree-level result at beam energies near  $M_Z$  [34, 35]. We calculate the background using NUNUGPV [34] which includes these QED radiative corrections.

Table 2 lists the maximum  $M_D$  sensitivity which can be reached at LEP2 from graviton production processes. We show results for two collider options: the recently completed run with  $\sqrt{s} = 190 \text{ GeV}$  and integrated luminosity  $\mathcal{L} = 4 \times 150 \text{ pb}^{-1}$ , and the near-future run

$\delta$	Max $M_D$	Max $M_D$
	sensitivity	sensitivity
	$\sqrt{s} = 190$ GeV $\mathcal{L} = 4 \times 150$ pb $^{-1}$	$\sqrt{s} = 200$ GeV $\mathcal{L} = 4 \times 500$ pb $^{-1}$
2	1100 GeV	1300 GeV
3	850	1000
4	700	800
5	600	650

Table 2: Maximum  $M_D$  sensitivity which can be reached by studying the final state  $\gamma + \cancel{E}$  at LEP2 with  $\sqrt{s} = 190$  GeV and integrated luminosity  $\mathcal{L} = 4 \times 150$  pb $^{-1}$ , or  $\sqrt{s} = 200$  GeV and integrated luminosity  $\mathcal{L} = 4 \times 500$  pb $^{-1}$ .

with perhaps  $\sqrt{s} = 200$  GeV and integrated luminosity  $\mathcal{L} = 4 \times 500$  pb $^{-1}$ . We define the statistically significant discovery to be

$$\sigma_{\text{Signal}} > 5 \frac{\sqrt{\sigma_{\text{Bkgd}} \mathcal{L}}}{\mathcal{L}}, \quad (86)$$

which is equal to 0.32 pb and 0.17 pb for the  $\sqrt{s} = 190$  and 200 GeV option, respectively. The relative fraction of background to signal is well within systematic errors, and so detecting a signal is statistically limited. With more luminosity one could probe higher values of  $M_D$ .

Here we have compared the signal of graviton production with the Standard Model background. However, the unknown physics at scales larger than  $M_D$  can produce other phenomena which can provide an unexpected source of background to the graviton signal. The effect of the ultraviolet physics can be absorbed in unknown coefficients of higher-dimensional local operators of the effective theory. For our considerations, dimension-six operators of the kind  $\bar{e}e\bar{\nu}\nu$  could be dangerous, as they would mimic the graviton signal. The effect of such an operator suppressed by  $M_D^2$  for the  $\gamma + \cancel{E}$  signature at a 1 TeV  $e^+e^-$  collider is shown in figs. 1 and 2 for a particular choice of chirality structure. Since the overall normalization of this operator is unknown, we cannot decide on its importance as a source of background. Studies at different  $\sqrt{s}$  and with different beam polarizations would be essential in discriminating between the signal from graviton production and the signal from higher-dimensional operators.

## 6.2 Hadron Colliders

We started our phenomenological analysis with the case of  $e^+e^-$  colliders because they allow a simpler discussion, as the fundamental process occurs at a fixed  $\sqrt{s}$ . We now illustrate the possibilities at the CERN LHC, which is an approved proton-proton collider capable of effectively studying the TeV physics region. The advantage of LHC is the large centre-of-mass energy available, but potential drawbacks are the smearing in the effective  $\sqrt{s}$  of parton collisions and the large Standard Model background.

The leading experimental signal of graviton production at the LHC is  $pp \rightarrow \text{jet} + \cancel{E}_T$  coming from the subprocess  $qg \rightarrow qG$  (which gives the largest contribution),  $q\bar{q} \rightarrow gG$ , and  $gg \rightarrow gG$ . The differential rates for these parton processes have been given in eqs. (64)–(66). The main background comes from processes with a  $Z$  boson and one jet in the final state, with the  $Z$  decaying into neutrinos. In hadron colliders we cannot isolate the  $Z$ -peak contribution and hence the background, as well as the signal, is given by two-body processes, in contrast with the case discussed in sect. 6.1. In figs. 3 we show the signal [36] and background [37] rates for transverse jet energy larger than  $E_{T,\text{jet}}^{\text{min}}$ , with an acceptance cut on the jet rapidity  $|\eta_{\text{jet}}| < 3$ . In this figure we have fixed  $M_D = 5$  TeV. In fig. 4 we show the  $M_D$  dependence for  $E_{T,\text{jet}}^{\text{min}} = 1$  TeV.

In hadron colliders the elementary scattering processes occur at different centre-of-mass energies. Therefore it is not straightforward to assess the applicability of the effective-theory approach. In order to quantify the ultraviolet sensitivity, we have plotted in figs. 3 and 4 two curves for each value of  $\delta$ . The first one, denoted by the symbol **a**, is the result of setting to zero the cross-sections in eqs. (64)–(66) whenever the effective centre-of-mass energy in the parton collision  $\sqrt{\hat{s}}$  is larger than  $M_D$ . The second curve, denoted by the symbol **b**, lets the cross-sections grow indefinitely with  $\sqrt{\hat{s}}$ . In the regions where the two curves almost coincide, the dominant contribution comes from momenta smaller than  $M_D$  and the effective theory is fully applicable. When the two curves go apart, the ultraviolet contributions become important, and our calculation is not under control.

The existence of a calculable perturbative region insensitive to the ultraviolet is related to the rapid decrease in parton luminosities with increasing  $\sqrt{\hat{s}}$  which more than compensates for the increase of the cross-sections in eqs. (64)–(66). The larger the value of  $\delta$ , the faster

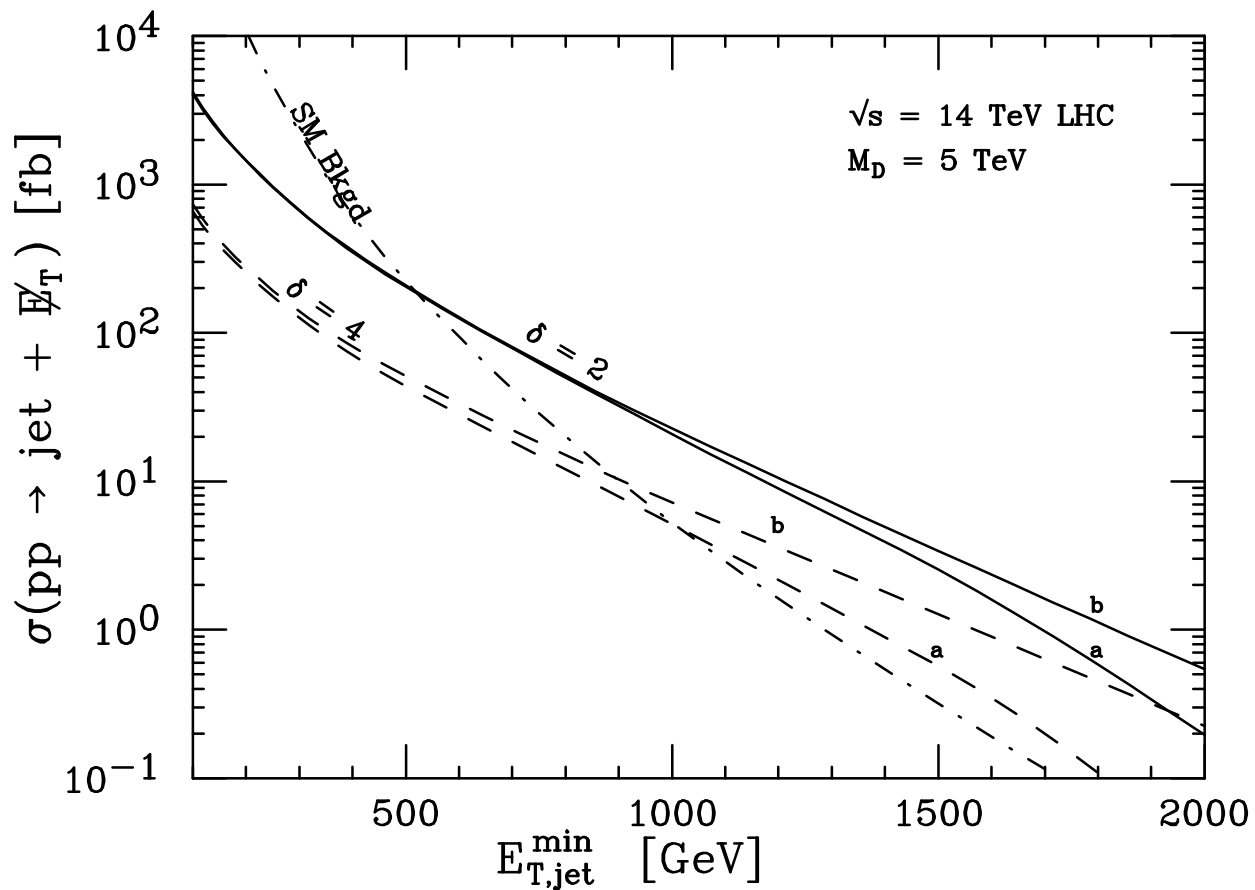


Figure 3: The total jet + nothing cross-section at the LHC integrated for all  $E_{T,\text{jet}} > E_{T,\text{jet}}^{\min}$  with the requirement that  $|\eta_{\text{jet}}| < 3.0$ . The Standard Model background is the dash-dotted line, and the signal is plotted as solid and dashed lines for fixed  $M_D = 5 \text{ TeV}$  with  $\delta = 2$  and 4 extra dimensions. The **a** (**b**) lines are constructed by integrating the cross-section over  $\hat{s} < M_D^2$  (all  $\hat{s}$ ).

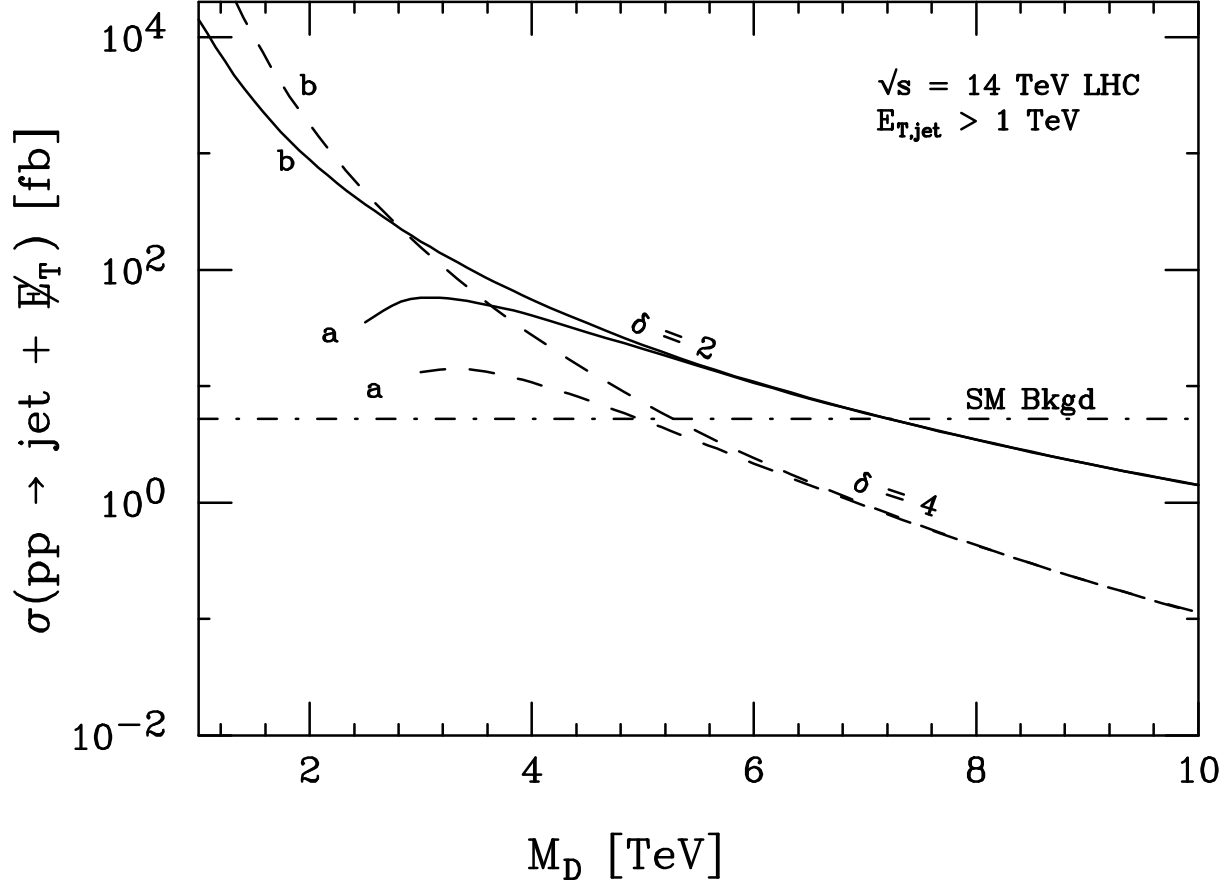


Figure 4: The total jet + nothing cross-section versus  $M_D$  at the LHC integrated for all  $E_{T,\text{jet}} > 1 \text{ TeV}$  with the requirement that  $|\eta_{\text{jet}}| < 3.0$ . The Standard Model background is the dash-dotted line, and the signal is plotted as solid and dashed lines for  $\delta = 2$  and 4 extra dimensions. The **a** (**b**) lines are constructed by integrating the cross-section over  $\hat{s} < M_D^2$  (all  $\hat{s}$ ).

the increase in the cross-section, and thus the sooner the non-perturbative region is reached, as shown in figs. 3 and 4.

In order to establish the LHC range of sensitivity, we consider two options for the integrated luminosity,  $\mathcal{L} = 10 \text{ fb}^{-1}$  and  $100 \text{ fb}^{-1}$ . We estimate the systematic error in the background prediction to be about 10%. This precision could be reached with a next-to-leading order calculation or by experimentally calibrating the background to the measured cross-section for jet +  $Z$ , with the  $Z$  decaying leptonically  $Z \rightarrow \ell^+ \ell^-$ .

For  $\mathcal{L} = 100 \text{ fb}^{-1}$ , the systematic error dominates, and the sensitivity range is defined by

$$\sigma_{\text{Signal}} > 5(10\%)\sigma_{\text{Bkgd}} = 2.6 \text{ fb.} \quad (87)$$

For  $\mathcal{L} = 10 \text{ fb}^{-1}$ , the systematic and statistical errors are comparable. We add them in quadrature and require

$$\sigma_{\text{Signal}} > \sqrt{2} \frac{5\sqrt{\sigma_{\text{Bkgd}}\mathcal{L}}}{\mathcal{L}} = 3.7 \text{ fb.} \quad (88)$$

The corresponding  $M_D$  sensitivity ranges are shown in table 3. These results are obtained using the curves of type **a**, which give a more conservative prediction of the signal. Table 3 also contains an estimate of the lower bound on  $M_D$  up to which the perturbative calculation presumably can be trusted. The criterion used is that the difference between curves **a** and **b** should be smaller than 50% of the result in curve **a**. It should be realized that by lowering  $E_{T,\text{jet}}^{\text{min}}$  the minimum value of  $M_D$  consistent with perturbativity is also lowered. Therefore, by adjusting the  $E_{T,\text{jet}}$  cut in experimental analyses, one can select different ranges of  $M_D$  to probe perturbatively. For  $\delta \geq 5$ , there is no region of  $M_D$  in which we can simultaneously trust perturbation theory and obtain a visible signal at LHC. Nevertheless, for  $\delta < 5$  the LHC probes perturbatively the multi-TeV region, which is prime territory if these ideas ameliorate the fine-tuning problem between the weak scale and the gravity scale. In the case of  $\delta = 2$ , the SN1987A bound discussed in sect. 6.1 rules out the possibility of an observable signal.

A different signal for graviton production comes from events with a photon and missing energy in the final state, arising from the subprocess  $\bar{q}q \rightarrow G\gamma$ . The Standard Model background originates mainly from  $\bar{q}q \rightarrow Z\gamma$ . Figures 5 and 6 show the results of the cross-section as a function of the cut on  $E_{T,\gamma}$  for a fixed  $M_D$ , and as a function of  $M_D$  for a fixed cut on  $E_{T,\gamma}$ , under the requirement  $|\eta_\gamma| > 2.5$ .

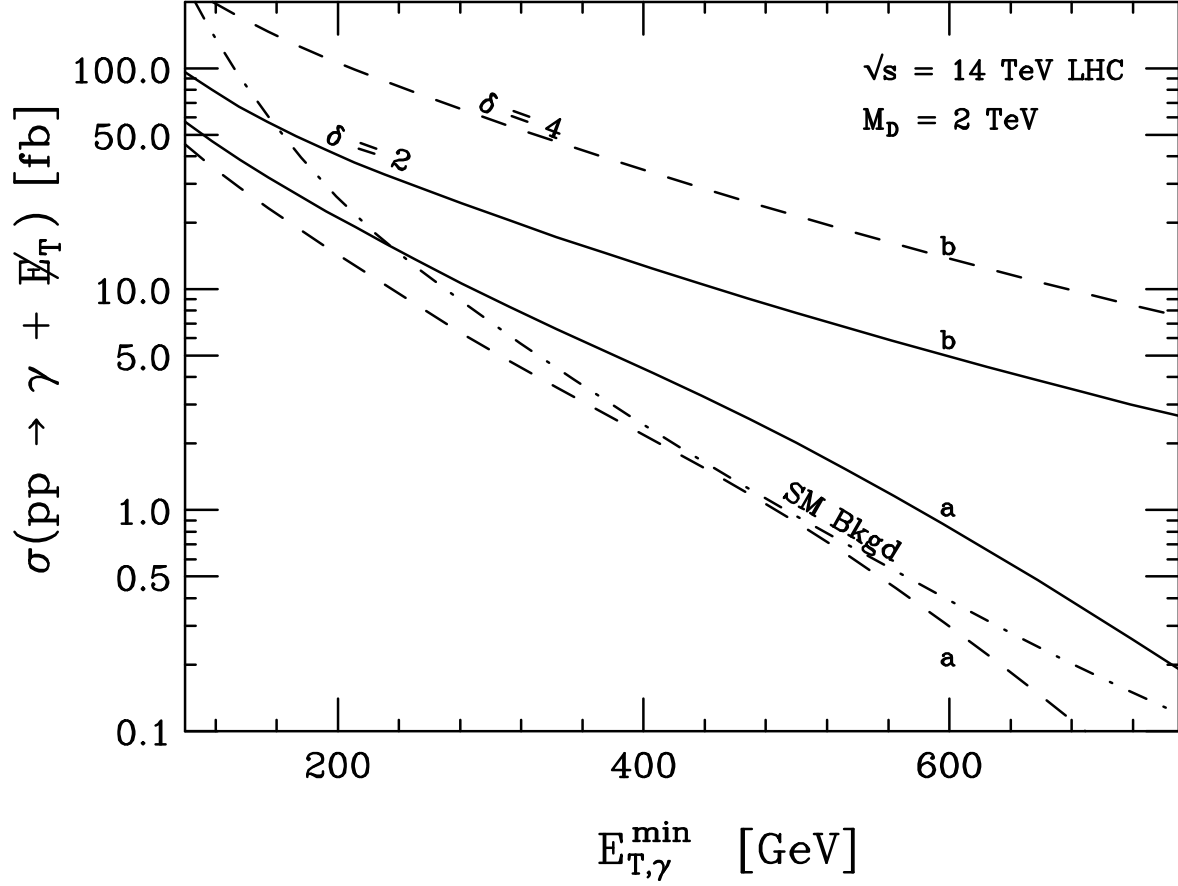


Figure 5: The total  $\gamma$  + nothing cross-section at the LHC integrated for all  $E_{T,\gamma} > E_{T,\gamma}^{\text{min}}$  with the requirement that  $|\eta_\gamma| < 2.5$ . The Standard Model background is the dash-dotted line, and the signal is plotted as solid and dashed lines for fixed  $M_D = 2$  TeV with  $\delta = 2$  and 4 extra dimensions. The **a** (**b**) lines are constructed by integrating the cross-section over  $\hat{s} < M_D^2$  (all  $\hat{s}$ ).

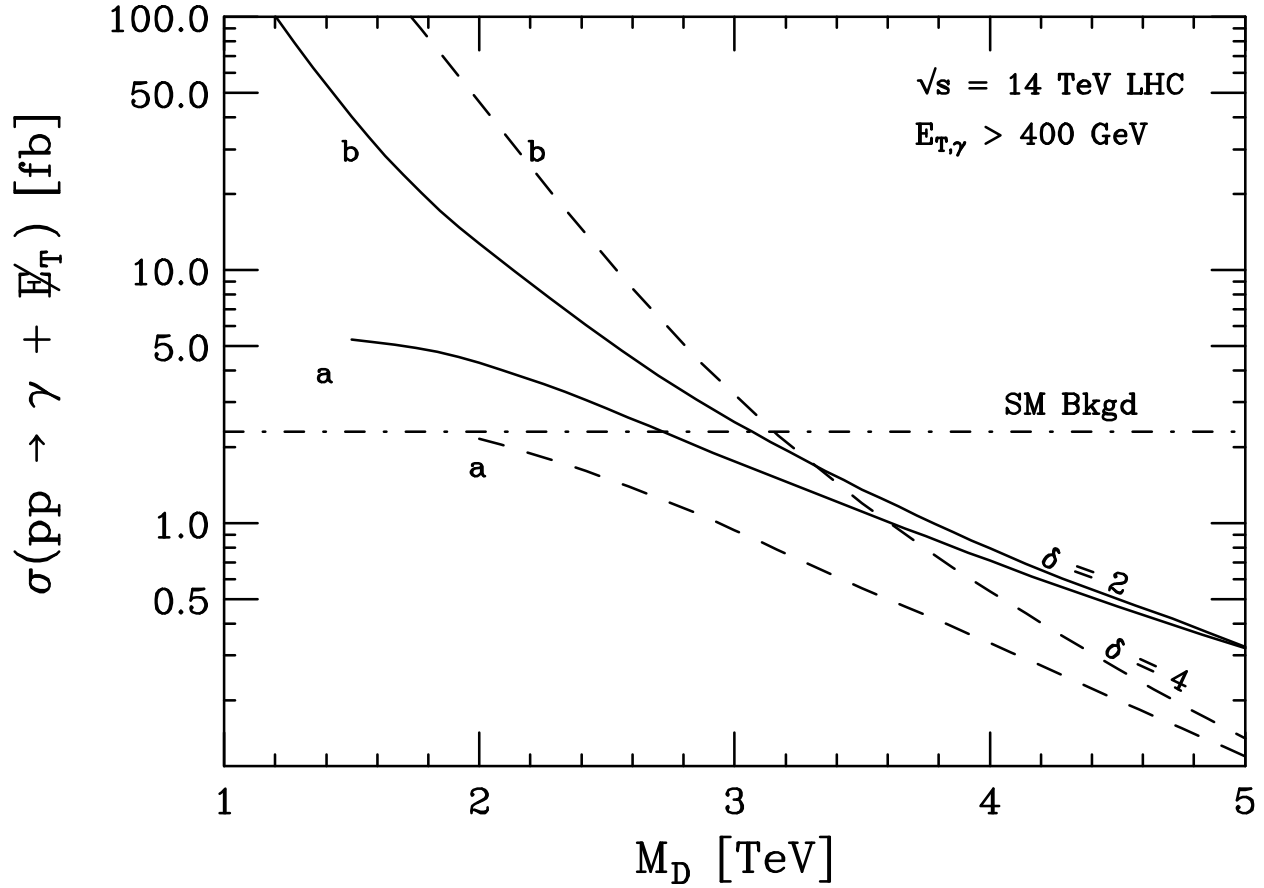


Figure 6: The total  $\gamma +$  nothing cross-section versus  $M_D$  at the LHC integrated for all  $E_{T,\gamma} > 400$  GeV with the requirement that  $|\eta_\gamma| < 2.5$ . The Standard Model background is the dash-dotted line, and the signal is plotted as solid lines for  $\delta = 2$  and 4 extra dimensions. The **a** (**b**) lines are constructed by integrating the cross-section over  $\hat{s} < M_D^2$  (all  $\hat{s}$ ).

$\delta$	Max $M_D$ sensitivity $\mathcal{L} = 100 \text{ fb}^{-1}$	Max $M_D$ sensitivity $\mathcal{L} = 10 \text{ fb}^{-1}$	Min $M_D$ perturbativity
2	8.5 TeV	7.9 TeV	3.8 TeV
3	6.8	6.3	4.3
4	5.8	5.5	4.8
5	5.0	4.6	5.4

Table 3: Maximum  $M_D$  sensitivity which can be reached by studying the final state jet+  $\cancel{E}_T$  at the LHC with  $\sqrt{s} = 14$  TeV and integrated luminosity  $\mathcal{L} = 100 \text{ fb}^{-1}$  or  $10 \text{ fb}^{-1}$ . The bounds have been obtained by requiring  $\sigma_{\text{Signal}} > 2.6 \text{ fb}$  (for  $\mathcal{L} = 100 \text{ fb}^{-1}$ ) or  $3.7 \text{ fb}$  (for  $\mathcal{L} = 10 \text{ fb}^{-1}$ ) with the acceptance cuts  $|\eta_{\text{jet}}| < 3$  and  $E_{T,\text{jet}} > 1 \text{ TeV}$ . We also give an estimate of the minimum value of  $M_D$  for which the effective-theory calculation can be trusted.

The disadvantage of the photon signal over the jet signal is the much lower rate, caused by the smallness of the electromagnetic coupling and the lower luminosity of  $\bar{q}q$  over  $qg$  at large values of  $\hat{s}/s$  in  $pp$  colliders. The lower rate requires smaller values of  $M_D$  to achieve a visible signal, and therefore a much more limited perturbative region. This is illustrated in figs. 5 and 6, since the curves **a** and **b** (defined as before) are significantly separated in most of the interesting region. Therefore, the sensitivity range of  $M_D$  obtained from the photon signal is much smaller than in the jet case. Nevertheless, in case of discovery in the jet channel, the photon signal can provide a useful independent test.

As discussed in sect. 6.1, other effects inherent to the full quantum-gravity theory can provide a source of background to the graviton signal. However, comparing to  $e^+e^-$  colliders, these effects could be less important here. First of all, there are no dimension-six operators contributing to<sup>¶</sup>  $qg \rightarrow qZ$ , or  $\bar{q}q \rightarrow gZ$ , or  $gg \rightarrow gZ$ . Moreover, dimension-six operators of the kind  $\bar{q}q\bar{\nu}\nu$  contribute only to processes with three-body final states, and should be less important than the two-body signal and background computed above.

We close this section by analysing the capabilities of the Tevatron in the jet+  $\cancel{E}_T$  mode. In fig. 7 we plot the cross-sections [36, 37] for  $p\bar{p} \rightarrow \text{jet} + \cancel{E}_T$  at  $\sqrt{s} = 2 \text{ TeV}$  as a function of  $E_{T,\text{jet}}^{\text{min}}$  with  $M_D = 1.2 \text{ TeV}$  fixed, and  $|\eta_{\text{jet}}| < 3$ . Here again, the signal is flatter with increasing  $E_{T,\text{jet}}^{\text{min}}$  than the background, and so it is helpful to go as high in  $E_T$  as is allowed

<sup>¶</sup>Operators of the kind  $\bar{f}\gamma_\mu D_\nu f F^{\mu\nu}$  vanish for massless fermions by the equations of motion.

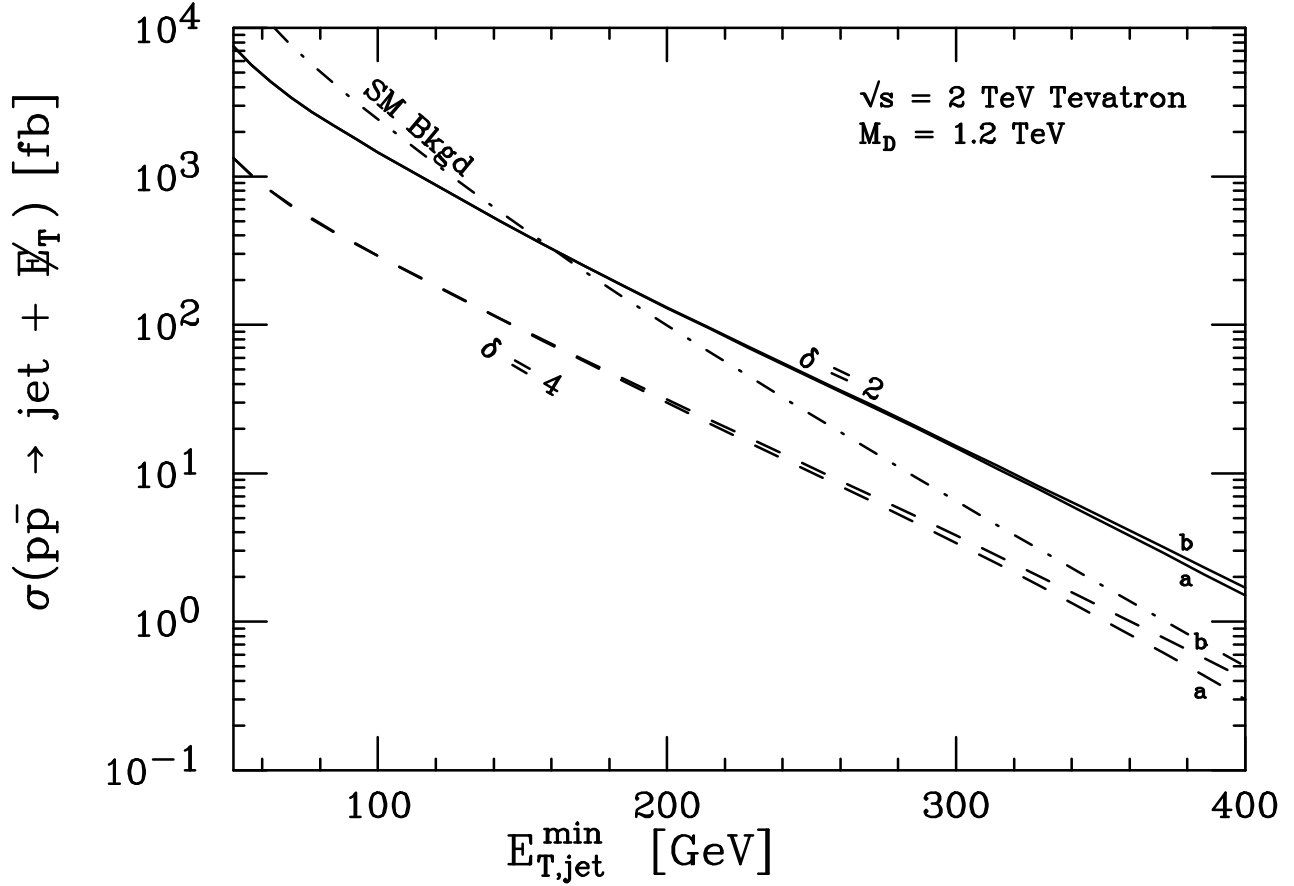


Figure 7: The total jet+nothing cross-section at the Tevatron ( $\sqrt{s} = 2 \text{ TeV}$ ) integrated for all  $E_{T,\text{jet}} > E_{T,\text{jet}}^{\min}$  with the requirement that  $|\eta_{\text{jet}}| < 3.0$ . The Standard Model background is the dash-dotted line, and the signal is plotted as solid and dashed lines for fixed  $M_D = 5 \text{ TeV}$  with  $\delta = 2$  and 4 extra dimensions. The **a** (**b**) lines are constructed by integrating the cross-section over  $\hat{s} < M_D^2$  (all  $\hat{s}$ ).

while still having enough events for a statistically significant signal. In fig. 8 we plot the  $M_D$  dependence of the jet+  $\cancel{E}_T$  cross-section for  $E_{T,\text{jet}}^{\text{min}} = 150$  GeV.

We calculate the  $M_D$  sensitivity at the Tevatron for two different centre-of-mass energies. For  $\sqrt{s} = 1.8$  TeV, with  $200 \text{ pb}^{-1}$  of integrated luminosity, and  $E_{T,\text{jet}}^{\text{min}} = 150$  GeV, the background is approximately 290 fb. Requiring a signal significance of  $S/\sqrt{B} = 5$ , we find  $\sigma_{\text{sig}} > 190$  fb for discovery. Note that this is statistics limited, since we assume that the background is known to better than about 10%. The resulting sensitivities of  $M_D$  are listed in table 4.

We carry out the same procedure to calculate sensitivities of  $M_D$  for a 2 TeV centre-of-mass Tevatron to be available for Run II. The background with  $E_{T,\text{jet}}^{\text{min}} = 150$  GeV is approximately 410 fb. The integrated luminosity for the next run is expected to be above several  $\text{fb}^{-1}$ ; however, the added luminosity helps little when  $E_{T,\text{jet}}^{\text{min}} = 150$  GeV, since we are limited by the systematic uncertainty in knowing the background cross-section. To take full advantage of the higher luminosity, one can choose a larger value of  $E_{T,\text{jet}}^{\text{min}}$  and gain increasing sensitivity to  $M_D$ , by enhancing the signal to background ratio. However, in this case, the minimum value of  $M_D$  from perturbativity requirements also increases and therefore, for our illustrative study, we prefer to keep  $E_{T,\text{jet}}^{\text{min}}$  fixed. If we assume that we will know the background cross-section to within 10%, either by theory or by inferring it from  $Z \text{ jet} \rightarrow l^+ l^- \text{ jet}$ , then confidence of a discovery will require that the signal be more than 50% of the background. This systematic uncertainty is the limiting factor in such searches provided the integrated luminosity is above  $300 \text{ pb}^{-1}$ , which is planned to be easily exceeded during Run II. In table 4 we give the  $M_D$  limits according to the preceding discussion, with  $E_{T,\text{jet}}^{\text{min}} = 150$  GeV, and find sensitivity to  $M_D$  above 1 TeV for  $2 \leq \delta \leq 4$ . For  $\delta = 5$  the signal is not large enough to be detectable in a purely perturbative regime.

## 7 The Operator $\mathcal{T}$ and Collider Experiments

As we have shown in sect. 5, the operator  $\mathcal{T}$  defined in eq. (71) is generated by a one-graviton exchange at tree level. Its coefficient in the interaction Lagrangian

$$\mathcal{L} = \frac{4\pi}{\Lambda_T^4} \mathcal{T} \tag{89}$$

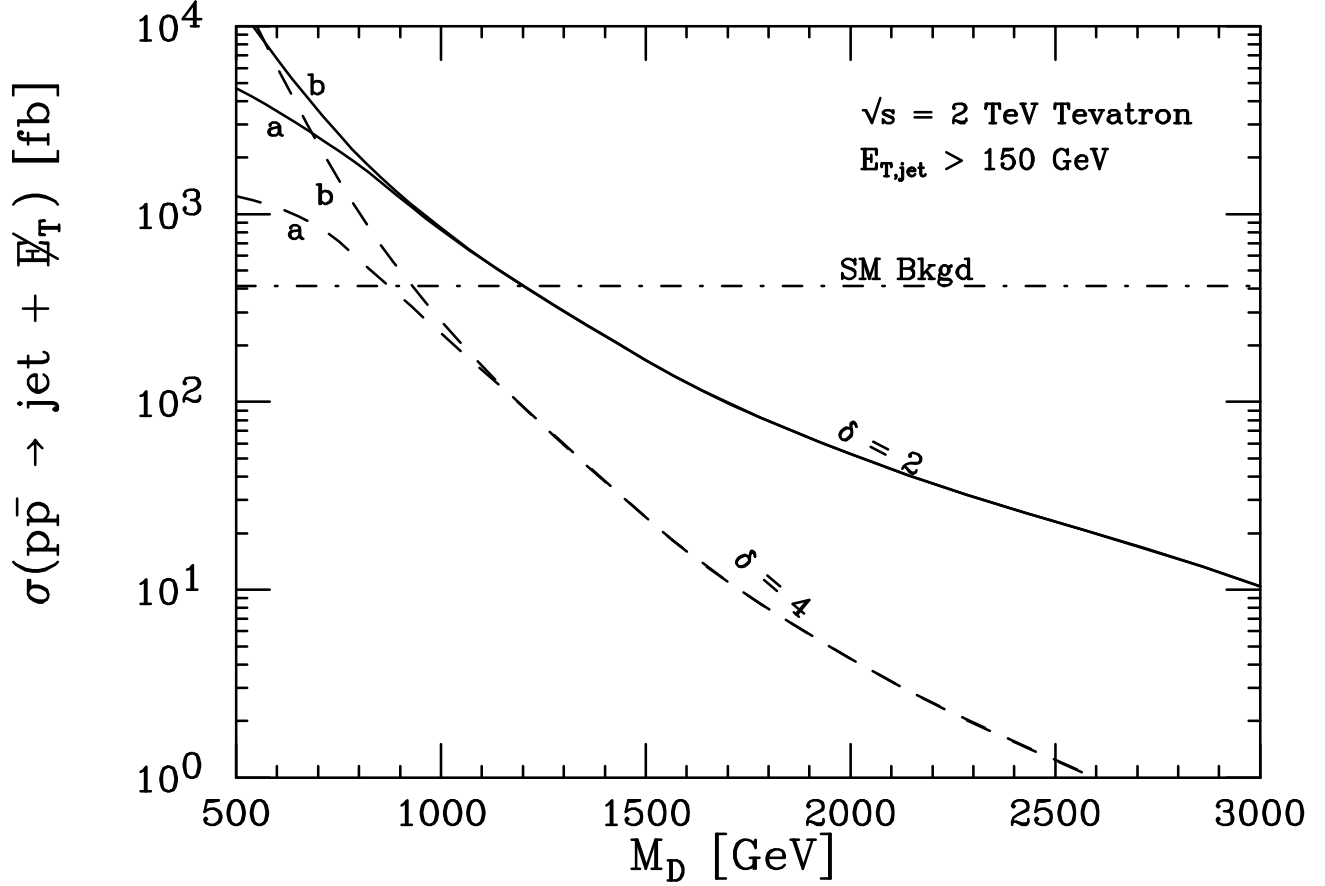


Figure 8: The total jet + nothing cross-section versus  $M_D$  at the Tevatron ( $\sqrt{s} = 2 \text{ TeV}$ ) integrated for all  $E_{T,\text{jet}} > 150 \text{ GeV}$  with the requirement that  $|\eta_{\text{jet}}| < 3.0$ . The Standard Model background is the dash-dotted line, and the signal is plotted as solid and dashed lines for  $\delta = 2$  and 4 extra dimensions. The **a** (**b**) lines are constructed by integrating the cross-section over  $\hat{s} < M_D^2$  (all  $\hat{s}$ ).

	Max $M_D$ sensitivity	Min $M_D$ perturbativity	Max $M_D$ sensitivity	Min $M_D$ perturbativity
$\delta$	$\sqrt{s} = 1.8 \text{ TeV}$ $\mathcal{L} = 200 \text{ pb}^{-1}$	$\sqrt{s} = 1.8 \text{ TeV}$	$\sqrt{s} = 2 \text{ TeV}$ $\mathcal{L} > 300 \text{ pb}^{-1}$	$\sqrt{s} = 2 \text{ TeV}$
2	1100 GeV	600 GeV	1400 GeV	650 GeV
3	950	700	1150	750
4	850	800	1000	850
5	700	900	900	950

Table 4: Maximum  $M_D$  sensitivity which can be reached by studying the final state jet+  $\cancel{E}_T$  at the Tevatron with  $\sqrt{s} = 1.8 \text{ TeV}$  and integrated luminosity  $\mathcal{L} = 200 \text{ pb}^{-1}$ , or  $\sqrt{s} = 2 \text{ TeV}$  and integrated luminosity  $\mathcal{L} > 300 \text{ pb}^{-1}$ . The bounds have been obtained by requiring  $\sigma_{\text{Signal}} > 190 \text{ fb}$  (for  $\sqrt{s} = 1.8 \text{ TeV}$ ) or  $205 \text{ fb}$  (for  $\sqrt{s} = 2 \text{ TeV}$ ) with the acceptance cuts  $|\eta_{\text{jet}}| < 3$  and  $E_{T,\text{jet}} > 150 \text{ GeV}$ . We also give an estimate of the minimum value of  $M_D$  for which the effective-theory calculation can be trusted.

is an ultraviolet-dependent unknown parameter, although the non-analytic energy dependence can be computed with the low-energy effective theory (see sect. 5). We will proceed on our phenomenological analysis assuming that  $\Lambda_T$  is an energy-independent parameter of order  $M_D$ .

Since the coefficient of the dimension-8 operator  $\mathcal{T}$  is sensitive to ultraviolet physics, it is certainly model dependent. However, we want to argue here that the operator  $\mathcal{T}$  has a special meaning. Although graviton loops (or other quantum-gravity effects) can produce any generic operator, even those of dimensions less than 8,  $\mathcal{T}$  is generated at tree level. If momenta integrals are cutoff at a scale equal to or less than  $M_D$ , the loop suppression may appear in the coefficients of the operators in the effective theory. Moreover, the operator  $\mathcal{T}$  gives a pure  $d$ -wave (spin two) contribution to certain scattering processes, a signature of the graviton existence. The same operator simultaneously gives contributions to several scattering processes, offering the possibility of testing gravitational universality. Finally, for certain processes, it is possible to show that no other operator of lower dimension can compete with  $\mathcal{T}$ . For all these reasons, we believe that it is phenomenologically interesting to focus briefly on experimental tests of  $\mathcal{T}$ .

## 7.1 $e^+e^-$ and Muon Colliders

The operator  $\mathcal{T}$  gives new contributions to Bhabha scattering in  $s$ ,  $t$ , and  $u$  channels. It gives pure  $d$ -wave contributions to  $e^+e^- \rightarrow \mu^+\mu^-$ , to vector boson production ( $e^+e^- \rightarrow \gamma\gamma, ZZ, W^+W^-$ ), and to processes with two-jet final states ( $e^+e^- \rightarrow \bar{q}q, e^+e^- \rightarrow gg$ ), three jets ( $e^+e^- \rightarrow \bar{q}qg, e^+e^- \rightarrow ggg$ ), and four jets ( $e^+e^- \rightarrow gggg$ ). Another interesting process is Higgs pair production  $e^+e^- \rightarrow HH$ , which has a cross-section independent of the electron Yukawa coupling. In absence of other operators, the deviations from the Standard Model predictions for all these processes are determined in terms of a single parameter  $\Lambda_T$ . In practice, it will be a highly non-trivial experimental task to disentangle many new contributions.

The most promising process is  $e^+e^- \rightarrow \gamma\gamma$ . Indeed, there are no operators of dimension less than 8 which can contribute at tree level to this process<sup>||</sup>. Therefore, observables associated with the two-photon final state may be good probes of  $\Lambda_T$ . Angular correlations of the photons with the electron have been used effectively to search for excited electron states contributing in the  $t$ -channel to  $e^+e^- \rightarrow \gamma\gamma$  [38]. A large composite electron mass in these studies is analogous to  $\Lambda_T$ . Therefore, the techniques employed to detect effects of compositeness can be directly applied to study effects of the local operator  $\mathcal{T}$  on  $e^+e^- \rightarrow \gamma\gamma$ .

A complete experimental study of this type would require scrutiny of the differential angular distribution of the photons. Binned counts of the photons produced at different angles are then compared statistically with the Standard Model expected distribution to detect anomalous behaviour. We do not present such a study here, but rather simplify the analysis to first plotting the integrated  $E_T$  spectrum of the photons, then choosing a value of  $E_{T,\gamma}^{\min}$  and comparing total counts expected in the Standard Model to those predicted for a given value of  $\Lambda_T$ .

In fig. 9 we plot the  $e^+e^- \rightarrow \gamma\gamma$  cross-section for different values of  $\Lambda_T$  as a function of  $E_{T,\gamma}^{\min}$  for a 1 TeV  $e^+e^-$  collider. As expected, the higher in  $E_{T,\gamma}$  we search, the more the signal wins over the background. If we require, for example, that  $E_{T,\gamma} > 300$  GeV, and also require for discovery that the total signal must be more than 10% of the background, we find sensitivity to  $\Lambda_T$  up to 3.8 TeV. This limit on  $\Lambda_T$  is independent of the number of extra

---

<sup>||</sup>The dimension-8 operator  $\bar{f}\gamma^\mu D_{\{\nu} D_{\lambda\}} f D_\nu F_{\mu\lambda}$  is independent of  $\mathcal{T}$  and contributes to  $e^+e^- \rightarrow \gamma\gamma$ . On the other hand, using the Bianchi identity, it can be shown that the operator  $\bar{f}\gamma^\mu f F^{\nu\lambda} D_\lambda F_{\mu\nu}$  vanishes under the equations of motion.

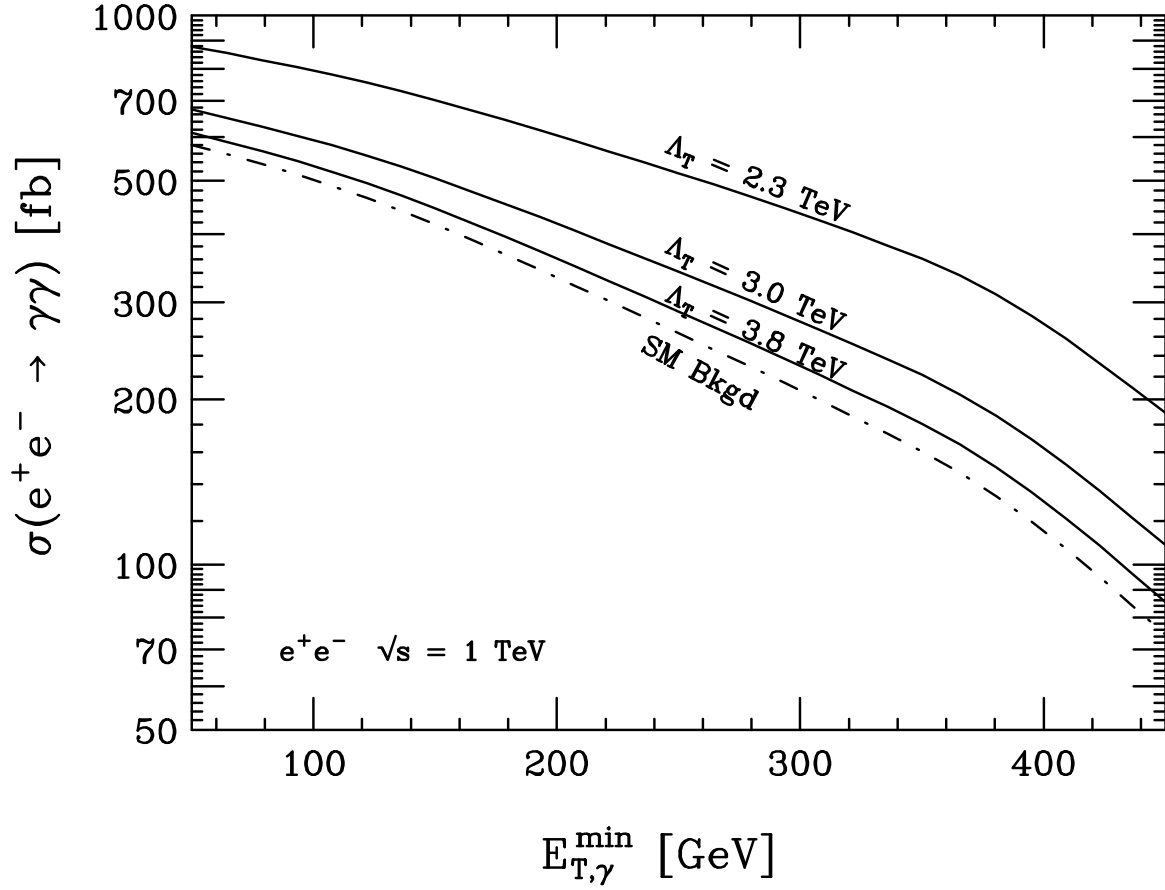


Figure 9: Total cross-section for  $e^-e^+ \rightarrow \gamma\gamma$  versus  $E_{T,\gamma}^{\min}$  at a 1 TeV centre-of-mass energy collider. The dashed line represents the Standard Model background, and the solid lines represent the total cross-section for various values of  $\Lambda_T$ .

dimensions; however, it should be noted that the relationship between  $\Lambda_T$  and  $M_D$  likely depends on  $\delta$  in an incalculable way.

Similar searches can also be performed at LEP. An interesting peculiarity is the study of virtual-graviton contributions to observables at the  $Z$  peak. Interference effects come only from imaginary parts and therefore from gravitons with masses equal to  $\sqrt{s}$ . These contributions can be computed reliably using the effective theory alone and can affect angular distributions of two-fermion final states. We estimate, however, that the searches for graviton production at LEP2 described in sect. 6.1 have better sensitivities to  $M_D$ .

## 7.2 Hadron Colliders

Similar to the case of  $e^+e^-$  colliders, the two-photon final state provides an interesting signal of the  $\mathcal{T}$  operator at hadron colliders. The  $\gamma\gamma$  final state has another advantage in the hadron collider environment: the measurable invariant mass of the two photons allows investigation of a possible signal in different energy domains (different  $\hat{s}$  regions), thereby enabling one to study the scaling behaviour of observables sensitive to virtual gravitons.

For the present, we show the effects of the operator  $\mathcal{T}$  on  $pp \rightarrow \gamma\gamma$  collisions by plotting in fig. 10 the integrated cross-section versus  $M_{\gamma\gamma}^{\min}$  for several values of  $\Lambda_T$ . This is done for the 14 TeV LHC, requiring  $|\eta_\gamma| < 2.5$  and  $E_{T,\gamma} > 50$  GeV for both photons. We find that the signal to background ratio is enhanced by going to higher  $M_{\gamma\gamma}^{\min}$ . However, keeping typical LHC luminosities in mind, we employ the cut  $M_{\gamma\gamma}^{\min} > 2$  TeV to our signal and background to make sure enough events are detectable. The Standard Model background is approximately 0.25 fb for this choice of  $M_{\gamma\gamma}^{\min}$ . With  $10 \text{ fb}^{-1}$  ( $100 \text{ fb}^{-1}$ ) we require 10 (50) signal events as discovery criteria, leading to sensitivity of  $\Lambda_T$  up to 5.8 TeV (7.1 TeV). Again, this limit is independent of the number of extra dimensions, but the relationship between  $\Lambda_T$  and  $M_D$  is likely not.

## 8 Conclusions

In this paper we have studied collider tests of the idea that gravity propagates in extra dimensions with very large radii [1]. Production of Kaluza-Klein excitations of the graviton

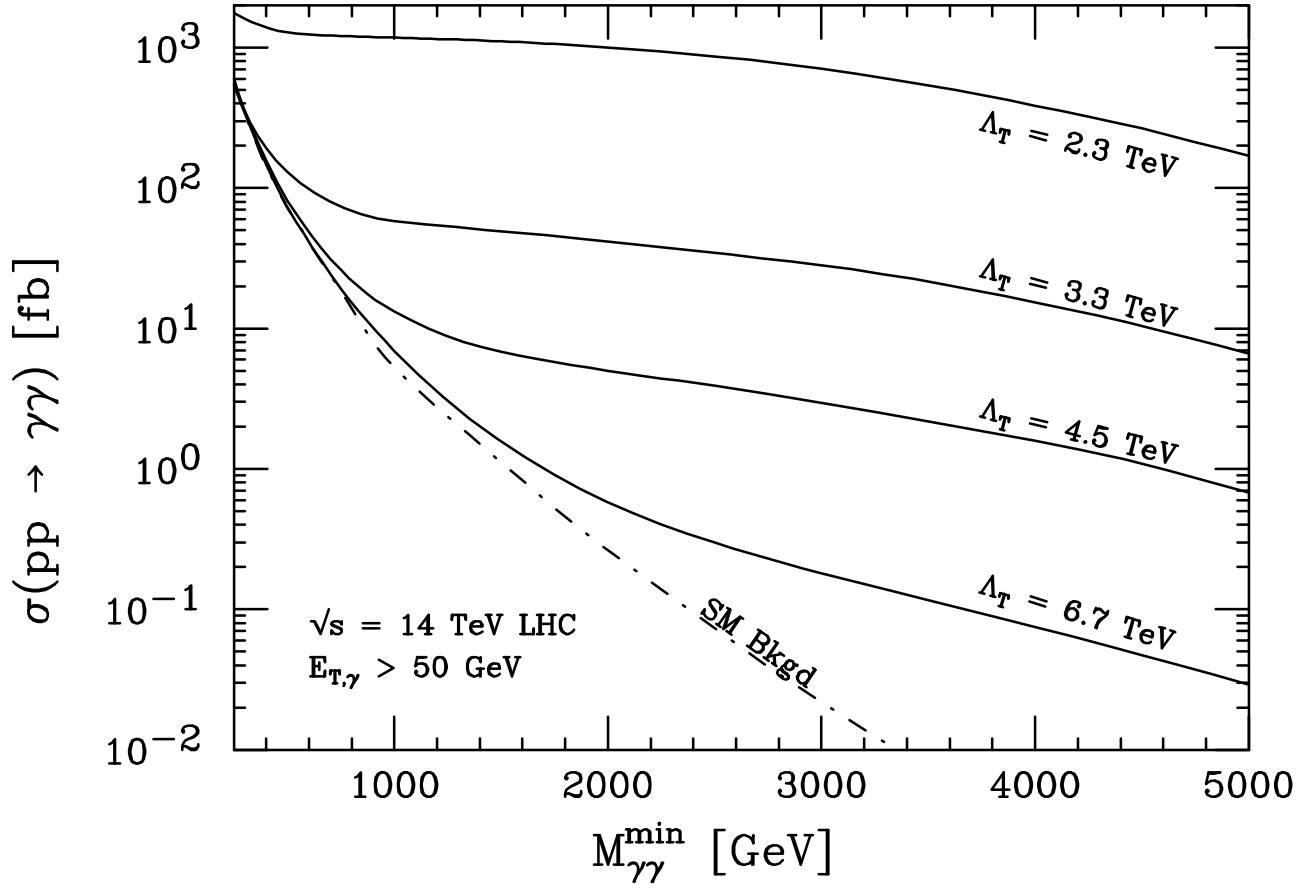


Figure 10: The total cross-section for  $pp \rightarrow \gamma\gamma$  integrated for  $\sqrt{\hat{s}} > M_{\gamma\gamma}^{\min}$  with the requirement that  $E_{T,\gamma} > 50$  GeV and  $|\eta_\gamma| < 2.5$  for each photon. The dashed line is the Standard Model background and the solid lines are the total cross-sections for various values of  $\Lambda_T$ .

can be predicted in a fairly model-independent way, using an effective Lagrangian approach. Here we have discussed the formalism to derive such an effective theory.

The basic collider signal of graviton production is missing energy, accompanied by a gauge boson or a hadronic jet. The graviton signal can be distinguished from other new-physics sources of similar events by studying different final-state topologies and kinematic distributions. Here we have discussed the discovery reach of LEP2, the Tevatron, the LHC, and future  $e^+e^-$  and muon colliders. It is worth emphasizing that the effective Lagrangian approach is valid only in a restricted energy window for which a signal is discernible. Therefore, the existence of various future high-energy colliders can be vital for this search, since the relevant energy window is different in different experiments. For instance, LHC could discover new physics phenomena specific to quantum gravity, and an  $e^+e^-$  collider could disentangle the many possible contributions to related signals, and measure the energy and angular dependent scalings of the graviton-induced cross-sections.

We have also studied simple scattering processes which receive contributions from virtual-graviton exchange at tree level. Deviations from Standard Model predictions could be an indication of the presence of Kaluza-Klein gravitons, although this signal is more model dependent.

The use of the effective theory is well justified in the infrared, but we cannot predict reliably the ultraviolet cutoff up to which we can extrapolate our results. At high energies, other unknown phenomena can appear and mimic our signal. Therefore, in the absence of anomalous events, our analysis can be directly applied to obtain lower bounds on the quantum-gravity scale. However, in case of discovery, careful experimental tests and studies of the correlations among new phenomena would need to be performed to obtain an understanding of the underlying theory. Nevertheless, it is very interesting that colliders originally planned to study the electroweak scale could give us direct information on the structure of quantum gravity.

*Acknowledgements:* We have greatly benefitted from discussions with S. Dimopoulos, M. Mangano, M. Moretti, M. Porrati, A. Signer, R. Sundrum, Z. Was, and A. Zaffaroni.

## Appendix

The  $F_i(x, y)$  functions are

$$F_1(x, y) = \frac{1}{x(y-1-x)} \left[ -4x(1+x)(1+2x+2x^2) + y(1+6x+18x^2+16x^3) - 6y^2x(1+2x) + y^3(1+4x) \right], \quad (90)$$

$$F_2(x, y) = -(y-1-x) F_1\left(\frac{x}{y-1-x}, \frac{y}{y-1-x}\right) = \frac{1}{x(y-1-x)} \left[ -4x(1+x^2) + y(1+x)(1+8x+x^2) - 3y^2(1+4x+x^2) + 4y^3(1+x) - 2y^4 \right], \quad (91)$$

$$F_3(x, y) = \frac{1}{x(y-1-x)} \left[ 1+2x+3x^2+2x^3+x^4 - 2y(1+x^3) + 3y^2(1+x^2) - 2y^3(1+x) + y^4 \right]. \quad (92)$$

The function  $F_1(x, y)$  determines the cross-section for  $f\bar{f} \rightarrow \gamma G$ . Because of QED invariance under charge conjugation,  $F_1(x, y)$  is invariant under exchange of the Mandelstam variables  $t$  and  $u$ . This is reflected in the property  $F_1(x, y) = F_1(y-1-x, y)$ . The same property holds also for the function  $F_3(x, y)$ , relevant to the QCD process.

The  $G_i(x)$  functions are,

$$G_1(x) = \left[ \frac{1+2x+2x^2}{-x(1+x)} \right]^{1/2}, \quad (93)$$

$$G_2(x) = \left[ \frac{-x}{16}(1+x)(1+2x+2x^2) \right]^{1/2}, \quad (94)$$

$$G_3(x) = 1+4x+6x^2+4x^3+2x^4, \quad (95)$$

$$G_4(x) = 1+10x+42x^2+64x^3+32x^4, \quad (96)$$

$$G_5(x) = 1+6x+12x^2+8x^3, \quad (97)$$

$$G_6(x) = 1+6x+6x^2, \quad (98)$$

$$G_7(x) = 9x^{-1}+22+24x+11x^2+x^3, \quad (99)$$

$$G_8(x) = 4+9x+6x^2+x^3, \quad (100)$$

$$G_9(x) = 9 + 18x + 15x^2 + 5x^3, \quad (101)$$

$$G_{10}(x) = 1 + 12x + 15x^2 + 5x^3, \quad (102)$$

$$G_{11}(x) = 40 + 114x + 126x^2 + 60x^3 + 9x^4. \quad (103)$$

The functions  $G_1, G_2, G_3, G_4, G_6$  are also invariant under exchange of  $t$  and  $u$  and therefore satisfy the property  $G_i(-1-x) = G_i(x)$ .

## References

- [1] N. Arkani-Hamed, S. Dimopoulos, and G. Dvali, Phys. Lett. B **429**, 263 (1998); preprint hep-ph/9807344.
- [2] J. Lykken, Phys. Rev. D **54**, 3693 (1996).
- [3] E. Witten, Nucl. Phys. B **471**, 135 (1996).
- [4] P. Horava and E. Witten, Nucl. Phys. B **460**, 506 (1996); Nucl. Phys. B **475**, 94 (1996).
- [5] I. Antoniadis, Phys. Lett. B **246**, 377 (1990).
- [6] P. Ginsparg, Phys. Lett. B **197**, 139 (1987).
- [7] K.R. Dienes, Phys. Rep. **287** (1997) 447.
- [8] S. Dimopoulos and G.F. Giudice, Phys. Lett. B **379**, 105 (1996); J.C. Long, H.W. Chan, and J.C. Price, preprint hep-ph/9805217.
- [9] V.A. Rubakov and M.E. Shaposhnikov, Phys. Lett. B **125**, 136 (1983).
- [10] J. Polchinski, preprint hep-th/9611050; C.P. Bachas, preprint hep-th/9806199.
- [11] I. Antoniadis, N. Arkani-Hamed, S. Dimopoulos, and G. Dvali, Phys. Lett. B **436**, 257 (1998).
- [12] G. Shiu and S.-H.H. Tye, preprint hep-th/9805157; Z. Kakushadze and S.-H.H. Tye, preprint hep-th/9809147.

- [13] A. Pomarol and M. Quiros, preprint hep-ph/9806263.
- [14] K.R. Dienes, E. Dudas, T. Gherghetta, and A. Riotto, preprint hep-ph/9809406.
- [15] K. Benakli, preprint hep-ph/9809582.
- [16] I. Antoniadis, S. Dimopoulos, A. Pomarol, and M. Quiros, preprint hep-ph/9810410.
- [17] D. Ghilencea and G.G. Ross, preprint hep-ph/9809217.
- [18] L. Randall and R. Sundrum, preprint hep-th/9810155.
- [19] C.P. Burgess, L.E. Ibañez, and F. Quevedo, preprint hep-ph/9810535.
- [20] R. Sundrum, preprint hep-ph/9807348.
- [21] N. Arkani-Hamed, S. Dimopoulos, and J. March-Russell, preprint hep-th/9809124.
- [22] K. Benakli and S. Davidson, preprint hep-ph/9810280.
- [23] I. Antoniadis, C. Muñoz, and M. Quiros, Nucl. Phys. B **397**, 515 (1993).
- [24] K.R. Dienes, E. Dudas, and T. Gherghetta, Phys. Lett. B **436**, 55 (1998); preprint hep-ph/9806292.
- [25] I. Antoniadis, K. Benakli, and M. Quiros, Phys. Lett. B **331**, 313 (1994).
- [26] R. Sundrum, preprint hep-ph/9805471.
- [27] A. Hashimoto and I.R. Klebanov, Phys. Lett. B **381**, 437 (1996).
- [28] I.R. Klebanov, Nucl. Phys. B **496**, 231 (1997); S.S. Gubser, I.R. Klebanov and A.A. Tseytlin, Nucl. Phys. B **499**, 217 (1997).
- [29] S. Weinberg, *Gravitation and Cosmology*, John Wiley & Sons, New York, 1972.

- [30] M.J.G. Veltman, “Quantum Theory of Gravitation” in *Methods in Field Theory*, Les Houches 1975, p. 265; S. Deser and P. van Nieuwenhuizen, Phys. Rev. D **10**, 401 (1974) and Phys. Rev. D **10**, 411 (1974); S. Deser, H.-S. Tsao, and P. van Nieuwenhuizen, Phys. Lett. B **50**, 491 (1974) and Phys. Rev. D **10**, 3337 (1974); F.A. Berends and R. Gastmans, Phys. Lett. B **55**, 311 (1975); M.T. Grisaru, P. van Nieuwenhuizen, and C.C. Wu, Phys. Rev. D **12**, 1813 (1975); A. Van Proeyen, Phys. Rev. D **15**, 2144 (1977) and Nucl. Phys. B **174**, 189 (1980).
- [31] For a related discussion in ordinary quantum gravity, see J.F. Donoghue, Lectures at the Advanced School on Effective Theories, Almunecar, Spain, June 1995, preprint gr-qc/9512024.
- [32] A. Brignole, F. Feruglio, and F. Zwirner, Nucl. Phys. B **516**, 13 (1998); A. Brignole, F. Feruglio, M.L. Mangano, and F. Zwirner, Nucl. Phys. B **526**, 136 (1998).
- [33] P.A. Baikov et al., in Proc. of X Workshop on High Energy Physics and Quantum Field Theory (QFTHEP-95), ed. by B. Levtchenko, V. Savrin, Moscow, 1996, p.101, preprint hep-ph/9701412; E.E. Boos, M.N. Dubinin, V.A. Ilyin, A.E. Pukhov, and V.I. Savrin, preprint hep-ph/9503280 .
- [34] G. Montagna, M. Moretti, O. Nicrosini, and F. Piccinini, preprint hep-ph/9807465.
- [35] A. Jacholkowska, J. Kalinowski, and Z. Was, preprint hep-ph/9803375.
- [36] The signal and background are calculated using the structure functions of M. Glück, E. Reya, and A. Vogt, Zeit. für Physik C **67**, 433 (1995).
- [37] The backgrounds at hadron colliders are calculated using PYTHIA: T. Sjöstrand, Comp. Phys. Comm. **82**, 74 (1994).
- [38] S. Kim et al. (AMY Collaboration), Phys. Lett. B **223**, 476 (1989); D. Decamp et al. (ALEPH Collaboration), Phys. Lett. B **236**, 501 (1990); B. Adeva et al. (L3 Collaboration), Phys. Lett. B **250**, 199 (1990); O. Adriani et al. (L3 Collaboration), Phys. Lett. B **288**, 404 (1992); M. Akrawy et al. (OPAL Collaboration), Phys. Lett. B **257**, 531 (1991); P. Abreu et al. (DELPHI Collaboration), Phys. Lett. B **433**, 429 (1998).